Electronic Properties of Complex Crystalline and Amorphous Phases of Ge and Si. II. Band Structure and Optical Properties*

J. D. Joannopoulos and Marvin L. Cohen
Department of Physics, University of California, Berkeley, California 94720
Inorganic Materials Research Division, Lawrence Berkeley Laboratory, Berkeley, California 94720
(Received 11 April 1973)

We present calculations of the band structures and the imaginary part of the dielectric function ϵ_2 as a function of energy for Ge and Si in the diamond, wurtzite, Si-III (BC-8) and Ge-III (ST-12) structures using the empirical pseudopotential method. In particular we have obtained the symmetries of wave functions along important symmetry directions and identified the major contributions to the optical structure. A further study is made into the optical properties of amorphous Ge and Si using our short-range-disorder model. We find that, unlike long-range-disorder models, short-range disorder can explain *both* the amorphous density of states and the amorphous ϵ_2. In particular we find that the ϵ_2 spectrum has the same form as an averaged matrix element as a function of frequency.

I. INTRODUCTION

In a previous[1] paper (hereafter referred to as I) we calculated the band structure and density of states of Ge and Si in the diamond (FC-2), wurtzite ($2H$-4),[2] Si-III (BC-8), and Ge-III (ST-12) structures using the empirical pseudopotential method (EPM). The trends observed with the increasing complexity of the structures indicated that short-range disorder (deviations in bond angles and bond lengths—which also provide for the presence of odd numbered rings—while all bonds are satisfied) was able to account well for the density of states of amorphous Ge and Si. This suggested that various distinctive features in the amorphous density of states[3] could be attributed to certain structural aspects of the amorphous phase. For example, deviations in the bond angles could be related to the shifting of states at the top of the valence band to higher energies for the amorphous case, and the presence of odd-numbered rings of bonds in ST-12 led us to an argument that suggests that fivefold and sevenfold rings of bonds are responsible for the introduction of states between the two s-like peaks in the amorphous density of states.

In this paper we are concerned with the spectra of the imaginary part of the dielectric function, ϵ_2, for the aforementioned structures. From a band-structure point of view we present a detailed analysis of the structure in ϵ_2 for Ge and Si in the $2H$-4, BC-8, and ST-12 cases along with their band structures containing the symmetries of wave functions along important directions. This is of interest since the BC-8 and ST-12 structures may have a variety of applications, e.g., exciton droplets and, when doped, superconductivity. From the point of view of understanding the amorphous phase the trends observed in ϵ_2 as the structures become more and more complex may give some insight into the amount of disorder necessary to produce the distinctive features of the amorphous ϵ_2. We shall show that our short-range-disorder model is the only theoretical model until now that can account for *both* the amorphous density of states and the amorphous ϵ_2.[4,5] In particular we shall show that when one measures the amorphous ϵ_2 spectrum one is essentially just measuring an averaged energy-dependent matrix element. The method of our calculations, the parameters used, and a description of the crystals studied were given in I and will not be repeated here.

In Sec. II we give a brief group-theoretical analysis of the crystals and a description of the notation used in labeling the band structures. In Sec. III we give an analysis of the ϵ_2 spectra. In Sec. IV we present and discuss results which are of interest to

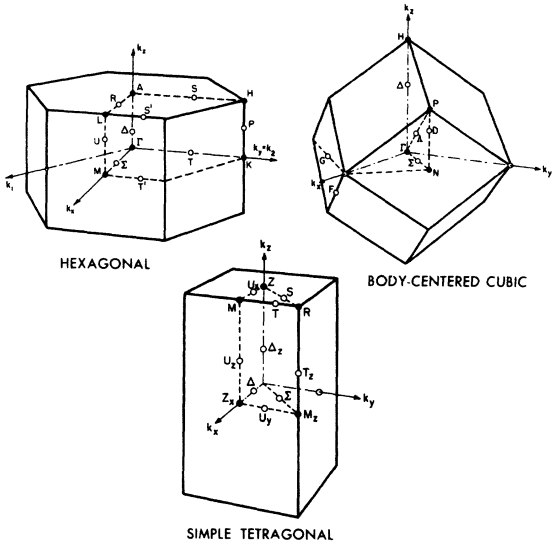

FIG. 1. Brillouin zones and associated symmetry points and lines for the $2H$-4, BC-8, and ST-12 structures.

the amorphous data. Finally, in Sec. V we make some concluding remarks. The reader interested only in the amorphous phase may proceed to Secs. IV and V with no loss in continuity.

II. SYMMETRY CONSIDERATIONS

We find that the $2H$-4 structure has a symmetry classification of D_{6h}^4 and is therefore associated with a nonsymmorphic space group. The BC-8 and ST-12 structures[6] have symmetry classifications T_h^7 and D_4^4, respectively, and are thus also associated with space groups which are nonsymmorphic. The Brillouin zones (BZ) for these structures are shown in Fig. 1 with the notation used by Leurhmann.[7] In order to label the symmetries of our wave functions, shown in Figs. 2, 4, 6, 8, 9 and 11, we have used the notation for point-group elements and the character tables found in Zak.[8] In our case, of course, these point operations must be followed by the appropriate translations. However, several remarks must be made relating to the additional symmetry, in some cases, demanded by time-reversal invariance, and to the symmetry notation for points located in the interior of the zone.

In the $2H$-4 (D_{6h}^4) structure, time-reversal invariance adds additional symmetry to R. Thus R_1 and R_2 in our notation are obtained from R_1+R_4 and R_2+R_3, respectively, using Zak's character table. In the case of M (D_{2h}) our notation is identified by replacing U^x and σ^x with U^1 and σ^1 in the character table for D_{2h} in Zak. For Σ (C_{2v}) we obtain our character table by replacing C_2, σ_v, and σ_v with U^1, σ, and σ^z, respectively, in the character table for C_{2v} in Zak. Similarly for Γ (D_{6h}) and Δ (C_{6v}) our notation is identified by replacing σ_h, $3\sigma_v$ with σ^z, $\sigma^{(x)}$ and $3\sigma_v$, $3\sigma_d$ with $3\sigma^{(x)}$, $3\sigma^{(1)}$, respectively, in the appropriate character tables found in Zak.

In the BC-8 (T_h^7) structure, time-reversal invariance adds additional symmetry to Λ, P, D, Γ, and H. Thus for Λ (C_3), Λ_1 and Λ_2 in our notation is obtained from 1 and 2+3, respectively, using Zak's character table. Similarly for P time-reversal invariance requires P_1 remain P_1 and P_2+P_3 becomes P_2. For D (C_2), D_1+D_2 becomes D_1 and for Γ (T_h), 1 becomes Γ_1, 2+3 becomes Γ_2, 4 becomes Γ_3, 5 becomes Γ_4, 6+7 become Γ_5, and 8 becomes Γ_6. The character table for H is the same as for T_h; it can be treated the same way as Γ. In the case of Δ (C_{2v}) our notation is identified by replacing C_2, σ_v, and σ_v with C_2^x, σ^y, and σ^z, respectively, in the character table for C_{2v} in Zak.

In the ST-12 (D_4^4) structure our notation regarding labeling of symmetry points and directions is that of Leuhrmann, as mentioned before, and for this case it differs from Zak's notation. Aside from this, time-reversal invariance requires that U^y, M^z, S, R, T, M, and U^z have additional symmetry. Thus Y_1+Y_2 using Zak's notation becomes U_1^y using our notation. Similarly for M^z, we have M_1 becomes M_1^z, M_2+M_3 become M_2^z, and M_4+M_5 become M_3^z, and for S we have S_1+S_2 become S. For R we have A_1+A_2 become R_1, and for T, T_1+T_2 become T_1. Finally for M we obtain M_1 from R_1+R_2 and M_2 from R_3+R_4, and for U^z we obtain U_1^z from W_1+W_2. In the case of $\Gamma(D_4)$, $\Delta(C_2)$, Σ (C_2), and Δ^z (C_4), which are internal symmetry points, our notation is identified using the character tables for D_4, C_2, C_2, and C_4, respectively, found in Zak.

III. BAND STRUCTURES AND OPTICAL SPECTRA

The band structures of Ge and Si in the $2H$-4, BC-8, and ST-12 structures, shown in Figs. 2, 4, 6, 8, 9, and 11, were obtained from EPM calculations and the form factors used were given in I. In Figs. 3, 5, 7, 10, and 12 we show the ϵ_2 spectra calculated from these band structures using

$$\epsilon_2(E)=\tfrac{1}{3}\frac{e^2\hbar^4}{\pi m^2E^2}\sum_{c,v}\int_{\mathrm{BZ}}\delta(E_c(\vec{k})-E_v(\vec{k})-E)\times|\langle\vec{k},c|\vec{\nabla}|\vec{k},v\rangle|^2d^3k\,, \qquad (1)$$

where $|\vec{k},v\rangle$ is a Bloch state in the valence band and the integral is over the entire BZ.

For the $2H$-4 and ST-12 structures we can distinguish between the polarization of the electric vector and the c axis taken to be in the z-direction. In this case the factor of $\frac{1}{3}$ in Eq. (1) is removed and we have parallel polarization if we use d/dz in the matrix element, and perpendicular polarization if we use d/dx or d/dy. The integration was performed using the Gilat-Raubenheimer scheme.[9] Tables I–VI summarize the major contributions to the various peaks in the ϵ_2 spectra for the six compounds. The first column identifies the energy of a particular peak and the second column contains the major contributions to this peak identified by interband transitions which are listed in order of decreasing strength. In particular, we list the bands which contribute more strongly once we are away from symmetry points and lines. The third column assigns the interband transitions to various regions of the BZ. Finally, in columns four and five we list the symmetries of the critical points and their associated energies, respectively. In some cases the symmetries were obtained from a preliminary analysis and warrant further investigation. These are designated in the tables by a tilde.

The complexity of the BC-8 and the ST-12 structures introduces the possibility that we may have critical points which are also inflection points along certain directions. Although it is rather difficult to determine this, it is conceivable that some of the critical points whose symmetries are uncertain may be of this type.

For completeness we present an analysis for all six compounds and although experimental optical

TABLE I. Theoretical ϵ_2 structure and identifications, including the location in the BZ, symmetry and energy of critical points for Ge and Si in the 2*H*-4 structure. Details are given in the text.

Ge 2*H*-4						Si 2*H*-4					
ϵ_2 peaks (eV)		Bands	Location in zone	Symmetry	Energy(eV)	ϵ_2 peaks (eV)		Bands	Location in zone	Symmetry	Energy(eV)
1.46	⊥	7,8-10	Γ_5-Γ_8	M_0	1.46	2.60	⊥	7-9	Σ_1-Σ_1 (0.3, 0, 0)	M_0	2.60
1.77	∥	6-10	Γ_1-Γ_8	M_0	1.77	2.60	∥	7-9	Σ_1-Σ_1		2.60
2.25	⊥	5-9	Γ_6-Γ_{10}	M_0	2.08	3.10	∥	7-9	(0.25, 0, 0.25)	M_0	3.02
			Δ_6-Δ_3		2.23	3.35	∥	7-9	U_2-U_2 (0.5, 0, 0.35)	M_1	3.34
		6-9	A_3-A_1	M_1	2.26	3.35	⊥	5-9	Γ_6-Γ_{10}	M_0	3.21
2.50	∥	7-9	(0.25, 0, 0.25)	M_0	2.48				Δ_6-Δ_3		3.31
2.50	⊥	8-10	Δ_5-Δ_1(0, 0, 0.3)	M_1	2.51			6-9	A_3-A_1	M_1	3.35
2.68	⊥	8-9	U_4-U_2 (0.5, 0, 0.35)	$\sim M_1$	2.68	3.60	⊥	8-10	Δ_5-Δ_1 (0, 0, 0.25)	M_1	3.59
2.75	∥	7-9	U_2-U_2 (0.5, 0, 0.4)	M_1	2.78	4.10	⊥	6-9	M_7-M_1		4.08
3.15	∥	7-10	(0.08, 0.08, 0.2)	M_0	3.03				Σ_4-Σ_1		4.09
		7-9	(0.11, 0.11, 0.2)	$\sim M_2$	3.14				U_3-U_1 (0.5, 0, 0.25)	M_2	4.11
3.35	⊥	6-9	(0.2, 0, 0.25)	M_1	3.35			7-9	R_2-R_1 (0.15, 0, 0.5)	M_2	4.13
3.57	∥	8-9	(0.2, 0.2, 0.35)	$\sim M_1$	3.57	4.25	∥	8-9	(0.2, 0.2, 0.35)	$\sim M_1$	4.21
3.60	⊥	6-9	M_7-M_1		3.61				H, S^1		4.26
			Σ_4-Σ_1		3.59	4.38	⊥	8-10	(0.2, 0, 0.4)	M_2	4.38
			U_3-U_1 (0.5, 0, 0.15)	$\sim M_2$	3.60				R_2-R_1 (0.2, 0, 0.5)		4.30
		8-10	(0.2, 0, 0.4)	M_2	3.80	4.68	∥	8-10	M, T^1	$\sim M_2$	4.64
			R_2-R_1 (0.25, 0, 0.5)		3.60			8-9	(0.3, 0.1, 0)	M_1	4.68
3.72	∥	8-9	(0.3, 0.3, 0.45)	M_1	3.72			7-11	(0.4, 0, 0.35)	M_0	4.61
4.52	⊥	8-11	L_2-L_1, U_4-U_2	$\sim M_0$	4.40			7-9	T(0.2, 0.2, 0)	$\sim M_2$	4.74
		8-9	T(0.23, 0.23, 0)	$\sim M_0$	4.45	4.69	⊥	8-9	T(0.2, 0.2, 0)	M_0	4.57
		7-11	(0.25, 0, 0.25)	$\sim M_1$	4.53			5,6-10	Δ_6-Δ_5 (0, 0, 0.3)	$\sim M_1$	4.69
4.52	∥	7-11	(0.25, 0, 0.25)	$\sim M_1$	4.53	4.89	⊥	7-9	K	$\sim M_2$	4.87
		8-9	K, T^1	M_2	4.52			8-9	(0.3, 0.25, 0.25)	$\sim M_2$	4.89
4.70	⊥	7-9	K, T^1	$\sim M_2$	4.67	4.91	∥	7-10	Σ(0.2, 0.08, 0)	$\sim M_2$	4.91
		8-9	(0.4, 0.15, 0.15)	M_3	4.72			8-10	(0.2, 0.1, 0)	$\sim M_2$	4.97
		8-12	A_3-A_3, S_1-S_1 (0.03, 0.03, 0.45)	$\sim M_2$	4.71	4.96	⊥	8-11	Σ (0.35, 0.05, 0.05)	$\sim M_2$	4.96
4.70	∥	8-11	M, T^1	M_0	4.67	5.50	⊥	8-14	Γ_5-Γ_{12}	M_1	5.47
		7-9	K, P (0.33, 0.33, 0.15)	$\sim M_3$	4.90	5.55	∥	8-12	M_5-M_4		5.61
5.23	⊥	8-14	Γ_5-Γ_{12}	M_2	5.23				Σ_3-Σ_4		5.54
		8-11	(0.08, 0.08, 0.35)	M_3	5.30						
5.29	∥	8-12	M_5-M_4		5.33						
			Σ_3-Σ_4		5.31						
		8-11	(0.3, 0.1, 0.15)		5.29						

TABLE II. Theoretical ϵ_2 structure and identifications, including the location in the BZ, symmetry and energy of critical points for Ge and Si in the BC-8 structure. Details are given in the text.

Ge BC-8					Si BC-8				
ϵ_2 peaks (eV)	Bands	Location in zone	Symmetry	Energy (eV)	ϵ_2 peaks (eV)	Bands	Location in zone	Symmetry	Energy (eV)
2.03	16-17	Σ_1-Σ_2 (0.37, 0.37, 0)	M_1	2.03	0.43	15,16-17	H_3-H_4	M_0	0.43
2.46	15-17	Σ_2-Σ_2 (0.4, 0.4, 0)		2.46	1.70	16-17	Δ_1-Δ_4 (0.55, 0, 0)	M_0	1.65
	13-17	Δ_4-Δ_4 (0.56, 0, 0)	M_0	2.41	2.04	16-17	(0.3, 0.55, 0)	$\sim M_2$	2.04
2.70	13-17	(0.2, 0.8, 0.15)	M_0	2.67	2.60	16-18	Σ_1-Σ_2 (0.4, 0.4, 0)	M_2	2.62
	14-18	G_2-G_1 (0.15, 0.15, 0)	$\sim M_0$	2.65		15-17	(0.3, 0.5, 0)	M_0	2.54
3.21	16-19	(0.25, 0.35, 0.25)	M_0	3.19	3.00	13-17	(0.2, 0.7, 0.15)	M_0	2.96
	13-17	G_1-G_2 (0.4, 0.6, 0)	M_2	3.24	3.45	13-17	(0.1, 0.5, 0.1)		3.46
		(0.3, 0.4, 0.15)		3.23		14-17	(0.2, 0.4, 0.15)	$\sim M_2$	3.45
	14-17	(0.2, 0.4, 0.15)	$\sim M_2$	3.21		16-19	(0.3, 0.4, 0.2)	M_1	3.43
	13-18	(0.3, 0.45, 0)	M_1	3.21		16-17	Γ_1-Γ_6	M_0	3.38
		G_1-G_1 (0.22, 0.78, 0)		3.23	3.70	13-17	G_1-G_2 (0.45, 0.55, 0)	M_2	3.70
3.76	15-19	N, G_2-G_1 (0.4, 0.55, 0)	M_3	3.78		15-19	D_1-D_1 (0.5, 0.5, 0.15)	M_1	3.68
	12-18	G_2-G_1 (0.35, 0.65, 0)	M_1	3.76	4.05	16-21	(0.2, 0.6, 0.15)		4.05
	15-17,18	Γ_2-Γ_6	M_3	3.74			Δ_1-Δ_2 (0.5, 0, 0)	M_2	4.04
3.98	14-19	(0.25, 0.65, 0.15)		4.00		15-21	(0.2, 0.6, 0.1)	M_0	4.02
4.50	12-19	(0.26, 0.63, 0.15)		4.50		13-18	G_1-G_1 (0.2, 0.8, 0)		4.02
	16-21	(0.15, 0.2, 0.1)	M_2	4.48		14-19	(0.25, 0.65, 0.1)	$\sim M_1$	4.07
	14-20	(0.1, 0.5, 0.1)		4.50	4.20	16-22	(0.2, 0.5, 0)	$\sim M_2$	4.20
	15-19	Δ_1-Δ_4 (0.25, 0, 0)	M_0	4.42		12-18	(0.15, 0.7, 0.15)	M_2	4.22
						15-22	(0.15, 0.7, 0)	M_0	4.14
					5.05	14-21	(0.2, 0.6, 0.1)	M_2	5.05
						13-20	D_1-D_1 (0.5, 0.5, 0.1)		5.00

TABLE III. Theoretical ϵ_2 structure, with perpendicular polarization, and identifications, including the location in the BZ, symmetry and energy of critical points for Ge ST-12. Details are given in the text.

Ge ST-12 $\vec{E} \perp \vec{c}$									
ϵ_2 peaks (eV)	Bands	Location in zone	Symmetry	Energy (eV)	ϵ_2 peaks (eV)	Bands	Location in zone	Symmetry	Energy (eV)
1.46	23,24-25	Σ_1-Σ_1 (0.35, 0.35, 0)	M_0	1.46		20-25	S_1-S_1 (0.06, 0.06, 0.5)	M_0	3.45
2.10	24-25	(0.4, 0.1, 0.3)	$\sim M_0$	2.08			S_1-S_1 (0.45, 0.45, 0.5)	$\sim M_1$	3.45
	23-25	(0.4, 0, 0.3)	M_1	2.18		17-25	T^z (0.5, 0.5, 0.3)	$\sim M_1$	3.53
2.55	24-26	(0.5, 0.1, 0.3)	M_1	2.48		24-27	(0, 0.1, 0.25)	$\sim M_2$	3.47
		T_1-T_1 (0.5, 0.5, 0.4)		2.52			T_1-T_1 (0.5, 0.3, 0.5)		3.50
		U_1^z-U_1^z (0.5, 0, 0.3)		2.50		20-26	T_1-T_1 (0.5, 0.35, 0.5)	M_2	3.47
	23-26	(0.4, 0.15, 0.25)		2.62		22-27	(0.3, 0.1, 0.3)	M_2	3.54
	22-25	(0.4, 0, 0.25)	$\sim M_2$	2.62			Δ_1-Δ_1 (0.45, 0, 0)		3.50
		M		2.60	3.65	17-25	(0.5, 0.25, 0.3)	M_2	3.67
	21-25	(0.4, 0.15, 0.25)	M_1	2.60			Z_1-Z_2,	M_0	3.65
	24-25	(0.1, 0.1, 0.4)	M_0	2.54		23-27	(0.1, 0, 0.25)		3.65
2.80	23,24-26	S_1-S_1 (0.4, 0.4, 0.5)	M_2	2.87		24-29	U^x (0.22, 0, 0.5)	M_0	3.60
	21-25	(0.4, 0.15, 0.25)	M_1	2.60		24-30	R_1-R_1	M_1	3.60
		Δ_1-Δ_1 (0.4, 0, 0)		2.80	4.20	24-30	U^x (0.3, 0, 0.4)		4.18
	24-25	U^x (0.2, 0, 0.4)	M_1	2.70			M		4.20
	24-27	(0.5, 0.1, 0.3)	M_1	2.76		21-27	(0.15, 0.15, 0.2)	M_2	4.22
		Γ_3-Γ_5	M_0	2.75		23-28	Δ_2-Δ_1 (0.1, 0, 0.05)		4.20
3.00	20-25	(0.4, 0.15, 0.25)	M_0	2.93		21-28	U^x (0.15, 0, 0.4)		4.20
	22-25	Z_2-Z_2	M_0	2.98		20-25	Σ_2-Σ_1 (0.07, 0.07, 0)	M_1	4.21
		T_1-T_1 (0.5, 0.5, 0.3)		3.00		23-32	S_1-S_1 (0.22, 0.22, 0.5)		4.20
	24-27	T^z (0.5, 0.5, 0.45)	M_1	3.11	4.50	23-31	U_1^z-U_1^z (0.5, 0, 0.2)	$\sim M_3$	4.57
	19-25	(0.35, 0.18, 0)		2.97		21-33	Σ_2-Σ_1 (0.4, 0.4, 0)		4.48
		M_2^z-M_1^z	$\sim M_2$	3.00		22-30	U^y (0.45, 0.1, 0.05)	M_1	4.36
	22-27	(0.5, 0.15, 0.3)	M_0	3.04			(0.3, 0.15, 0.4)	M_1	4.52
3.20	24-27	Z_1-Z_1	M_0	3.18		20-26	(0.15, 0, 0.1)	M_3	4.54
		Z_1^z-Z_1^z	M_3	3.20		20-28	(0.15, 0.15, 0.25)	M_0	4.47
	21-25	U^x (0.2, 0, 0.5)	M_2	3.21		14-27	M_3^z-M_1^z		4.46
	23-28	R, T^z	$\sim M_1$	3.20		23-34	Σ_1-Σ_1 (0.36, 0.36, 0)		4.48
	19-25	(0.5, 0.15, 0.3)	M_2	3.21		23-35	Σ_1-Σ_2 (0.35, 0.35, 0)		4.48
		Δ_1-Δ_1 (0.38, 0, 0)		3.20		21-29	Δ_3^z-Δ_1^z (0, 0, 0.22)		4.50
3.50	19-25,26	R_1-R_1	M_0	3.46		22-31	Δ_1^z-Δ_4^z (0, 0, 0.3)		4.50
	18-25	T_1-T_1 (0.5, 0.22, 0.5)	$\sim M_0$	3.49		24-33	U_1^y-U_1^y (0.5, 0.2, 0)		4.52

TABLE IV. Theoretical ϵ_2 structure, with parallel polarization, and identifications, including the location in the BZ, symmetry and energy of critical points for Ge ST-12. Details are given in the text.

Ge ST-12 $\vec{E} \parallel \vec{c}$									
ϵ_2 peaks (eV)	Bands	Location in zone	Symmetry	Energy (eV)	ϵ_2 peaks (eV)	Bands	Location in zone	Symmetry	Energy (eV)
1.60	24-25	Σ_2-Σ_1 (0.35, 0.35, 0)	M_0	1.46			U_1^z-U_1^z (0.5, 0, 0.2)		3.71
		Δ_2-Δ_1 (0.4, 0, 0)	$\sim M_1$	1.70	3.90	19-25	(0.2, 0.15, 0.3)	M_3	3.92
2.15	21-25	Σ_2-Σ_1 (0.37, 0.37, 0)	M_0	2.07		24-29	Δ_2^z-Δ_2^z (0, 0, 0.18)	M_2	3.94
	24-25	(0.4, 0.1, 0.3)	$\sim M_0$	2.08		23-29	Δ_1-Δ_2 (0.37, 0, 0)	$\sim M_2$	3.90
	23-25	(0.4, 0, 0.3)	M_1	2.18			S_1-S_1 (0.26, 0.26, 0.5)		3.90
2.65	21-25	(0.4, 0.15, 0.25)	M_1	2.60		21-26	Δ_2-Δ_1 (0.15, 0, 0)	$\sim M_1$	3.88
		Z_1^x-Z_1^x	$\sim M_2$	2.65	4.20	24-29	Γ_3-Γ_4	M_3	4.22
		U_1^y-U_1^y		2.63		20-25	Γ_3-Γ_4	M_0	4.16
	22-26	(0.5, 0.2, 0.25)	M_1	2.74			Σ_2-Σ_1 (0.07, 0.07, 0)	M_1	4.21
	22-25	M_3^z-M_1^z	$\sim M_2$	2.70		21-28	Γ_2-Γ_1	M_0	4.22
	24-25	Γ_3-Γ_4	M_0	2.64			Δ_1^z-Δ_1^z		4.23
3.20	24-27	Z_1-Z_1	M_0	3.18			U^x (0.15, 0, 0.4)		4.20
		Z_1^x-Z_1^x	M_3	3.20			S_1-S_1 (0.25, 0.25, 0.5)		4.20
		Δ_2-Δ_1 (0.45, 0, 0)	$\sim M_2$	3.18		22-29	(0.15, 0.15, 0.2)	M_0	4.21
	21-25	U^x (0.2, 0, 0.5)	M_2	3.21			Z_1^x-Z_1^x	M_2	4.24
		(0.2, 0.2, 0.3)		3.20		24-30	(0.1, 0.1, 0.3)	M_1	4.26
	24-26	S_1-S_1 (0.26, 0.26, 0.5)	M_3	3.26		22-30	(0.3, 0.25, 0.25)		4.21
	23-28	R_1-R_1		3.20	4.40	20-26	(0.17, 0.17, 0.1)	M_2	4.42
	24-28	Σ_2-Σ_1 (0.25, 0.25, 0)	$\sim M_1$	3.20		18-27	Z_1-Z_1	M_0	4.36
3.50	20-25	Z_2-Z_2		3.48		22-28	Σ_2-Σ_1 (0.14, 0.14, 0)		4.40
		S_1-S_1 (0.06, 0.06, 0.5)	M_0	3.45		22-27	Σ_1-Σ_2 (0.14, 0.14, 0)		4.37
	22-27	(0.3, 0.1, 0.3)	M_2	3.54			Δ_1-Δ_2 (0.25, 0, 0)		4.40
		Γ_5-Γ_5	M_0	3.44		23-34	M_2^z-M_1^z	$\sim M_2$	4.40
	20-26	(0.3, 0.1, 0.3)		3.53			Σ_1-Σ_2 (0.35, 0.35, 0)		4.40
	24-29	Σ_2-Σ_1 (0.35, 0.35, 0)		3.45		16-26	Z_2-Z_2	$\sim M_1$	4.37
	24-26	Δ_1-Δ_2 (0.3, 0, 0)		3.48			Δ_2^z-Δ_3^z		4.40
3.70	24-28	Δ_1-Δ_2 (0.26, 0, 0)		3.70		23-30	(0.35, 0.15, 0.3)	M_3	4.42
		S_1-S_1 (0.2, 0, 0)	$\sim M_2$	3.70			Δ_1-Δ_2 (0.37, 0, 0)		4.40
	21-27	Z_1^x-Z_1^x	M_1	3.69		22-31	U_1^y-U_1^y (0.5, 0.3, 0)		4.40

TABLE V. Theoretical ϵ_2 sturcture, with perpendicular polarization, and identifications, including the location in the BZ, symmetry and energy of critical points for Si ST-12. Details are given in the text.

Si ST-12 $\vec{E}\perp\vec{c}$									
ϵ_2 peaks (eV)	Bands	Location in zone	Symmetry	Energy (eV)	ϵ_2 peaks (eV)	Bands	Location in zone	Symmetry	Energy (eV)
1.76	24-25	(0.4, 0.2, 0)	M_0	1.76	3.60	20-25	z, U^x (0.1, 0, 0.5)	M_0	3.60
2.33	23-25	(0.4, 0, 0.3)	M_0	2.31		21-26	(0.3, 0.2, 0.25)	$\sim M_1$	3.60
	24-25	(0.4, 0, 0.45)	M_1	2.33		22-27	Σ_2-Σ_1 (0.3, 0.3, 0)	M_0	3.50
2.50	23,24-26	M	$\sim M_1$	2.50		21-29	R_1-R_1	M_0	3.59
		T_1-T_1 (0.5, 0.15, 0.5)	M_1	2.52		23-27	(0.1, 0.1, 0.25)	M_0	3.54
		U_1^x-U_1^x		2.51		23-28	(0.5, 0.15, 0.3)	M_1	3.58
		z^x, U_1^y-U_1^y		2.45		22-26	Δ_2^x-Δ_4^x (0, 0, 0.3)		3.60
2.80	23,24-26	S_1-S_1 (0.4, 0.4, 0.5)		2.76		22-28	Σ_2-Σ_1 (0.32, 0.32, 0)		3.60
		(0.4, 0.4, 0.4)	M_1	2.80	3.85	24-29	z_1^x-z_1^x	M_1	3.92
	21-25	(0.45, 0.15, 0.3)	M_0	2.73		23-28	Γ_5-Γ_1	M_0	3.71
		Δ_2-Δ_1 (0.45, 0, 0)		2.80			Δ_4^x-Δ_1^x (0, 0, 0.24)	M_2	3.85
	21-25 }	U_1^y-U_1^y (0.5, 0.2, 0)	M_1	2.79		23-29	(0.35, 0.15, 0.25)		3.85
	22-26 }	(0.5, 0.3, 0.15)		2.82		17-25	U_1^x-U_1^x (0.5, 0, 0.33)		3.85
	23-28	z_1-z_1	M_0	2.78		22-27	(0.15, 0.15, 0.2)	$\sim M_1$	3.81
	22-25	(0.4, 0, 0.25)	M_2	2.74		21-29	Σ_1-Σ_2 (0.42, 0.42, 0)	M_1	3.88
3.20	20-25	Δ_1-Δ_1 (0.39, 0, 0)	M_0	3.17		20-26	(0.15, 0.1, 0.4)	$\sim M_1$	3.89
		Σ_1-Σ_1 (0.37, 0.37, 0)	M_2	3.21		16-25	M_3^x-M_2^x	M_1	3.86
	19-25	Σ_2-Σ_2 (0.4, 0.4, 0)	$\sim M_1$	3.18		23-30	(0.35, 0.35, 0.25)	$\sim M_1$	3.81
	22-25	Z_2-Z_2	M_0	3.18	4.45	20-26	(0.1, 0, 0.1)	$\sim M_2$	4.48
		(0.2, 0.2, 0.25)	M_1	3.16			Σ_1-Σ_1 (0.12, 0.12, 0)		4.44
	20-26	U^y (0.5, 0.35, 0.05)	M_1	3.17		23-35	M_2^x-M_3^x		4.46
		Σ_1-Σ_1 (0.4, 0.4, 0)		3.20		15-27 }	M_3^x-M_1^x	$\sim M_1$	4.45
	22-28	U_1^y-U_1^y (0.5, 0.4, 0)		3.20		15-26 }	Σ_2-Σ_1 (0.44, 0.44, 0)		4.42
		R_1-R_1		3.20			U_1^x-U_1^x (0.5, 0, 0.34)		4.45
	21-26	T^z (0.5, 0.5, 0.4)	M_2	3.23		14-26	M_3^x-M_2^x		4.41
3.38	20-25	R, T^z (0.5, 0.5, 0.45)	M_1	3.39			T_1-T_1 (0.5, 0.28, 0.5)		4.45
	19-25	R, T^z (0.48, 0.48, 0.4)	$\sim M_3$	3.45		21-27	(0.2, 0, 0.2)	$\sim M_1$	4.40
		Σ_1-Σ_1 (0.35, 0.35, 0)		3.35			Δ_3^x-Δ_2^x (0, 0, 0.27)		4.45
	22-26	(0.25, 0.25, 0.3)	$\sim M_2$	3.36		22-33	Σ_2-Σ_1 (0.44, 0.44, 0)		4.45
	18-25	(0.4, 0.2, 0)	M_0	3.35			Σ_1-Σ_1 (0.4, 0.4, 0)		4.45
		U_1^y-U_1^y (0.5, 0.38, 0)		3.40		19-27	(0.35, 0.15, 0.3)	M_2	4.48
	24-27	(0.15, 0, 0.3)	M_1	3.38		21-28	Δ_3^x-Δ_1^x (0, 0, 0.24)		4.43
		U_1^x-U_1^x (0.5, 0, 0.15)		3.38		22-29	U_1^y-U_1^y (0.5, 0.11, 0)		4.41
	22-28	z_2-z_1	M_0	3.37		19-25	Σ_2-Σ_1 (0.15, 0.15, 0)		4.45
		(0.45, 0.4, 0.3)	M_1	3.35		17-28	M		4.42

TABLE VI. Theoretical ϵ_2 structure, with parallel polarization, and identifications, including the location in the BZ, symmetry and energy of critical points for Si ST-12. Details are given in the text.

				Si ST-12 $\vec{E} \parallel \vec{c}$					
ϵ_2 peaks (eV)	Bands	Location in zone	Symmetry	Energy (eV)	ϵ_2 peaks (eV)	Bands	Location in zone	Symmetry	Energy (eV)
1.76	24-25	(0.4, 0.2, 0)	M_0	1.76	3.90	24-30	(0.5, 0.22, 0.25)	M_1	3.92
2.32	23-25	(0.4, 0, 0.3)	M_0	2.31		24-29,30	Z_1^x-Z_1^x	M_0	3.93
	24-25	(0.4, 0, 0.45)	M_1	2.33			U_1^y-U_1^y		3.95
	24-26	U_1^z-U_1^z (0.5, 0, 0.4)	M_0	2.46		24-29	Γ_3-Γ_4	M_2	3.98
	22-25	Σ_2-Σ_1 (0.35, 0.35, 0)	M_0	2.32		23-29	(0.2, 0, 0.3)	M_0	3.91
2.80	24-26	(0.1, 0.1, 0.4)	M_0	2.81		18-25	(0.3, 0, 0.4)		3.90
		(0.2, 0.2, 0.5)	M_0	2.79			Δ_2-Δ_1 (0.35, 0, 0)		3.90
	21-25	(0.45, 0.15, 0.3)	M_0	2.73		21-26	Σ_2-Σ_1 (0.16, 0.16, 0)	M_1	3.92
	21-25 }	U_1^y-U_1^y (0.5, 0.2, 0)	M_1	2.78		22-30	(0.35, 0.35, 0.1)	M_0	3.81
	22-26 }	(0.5, 0.3, 0.15)		2.82		23-28	Δ_2^z-Δ_2^z(0, 0, 0.22)		3.88
		M	M_0	2.65	4.26	20-25	Γ_3-Γ_4	M_0	4.07
	24-27	Z_1-Z_1	M_0	2.79		22-29	M	$\sim M_1$	4.28
	24-25	(0.2, 0.05, 0.4)	M_2	2.81		22-32	M_3^z-M_3^z		4.30
3.30	21-25	U^z (0.2, 0, 0.5)	M_2	3.33			U_1^y-U_1^y (0.5, 0.3, 0)		4.26
	23-27	(0.35, 0.15, 0.3)	M_1	3.31		20-28	(0.4, 0.2, 0.25)		4.30
	22-26	(0.25, 0.25, 0.3)	$\sim M_2$	3.36		18-27	Z_1-Z_1	M_1	4.25
	23-26	Γ, Δ_4^z-Δ_4^z		3.30		24-30	U_1^z-U_1^z (0.5, 0, 0.15)		4.26
	24-26	(0.12, 0.12, 0.25)	M_2	3.25			S_1-S_1 (0.3, 0.3, 0.5)		4.27
	21-28	Σ_2-Σ_1 (0.4, 0.4, 0)		3.30			Δ_1-Δ_2 (0.36, 0, 0)		4.26
3.65	22-27	Z, S (0.15, 0.1, 0.45)	$\sim M_1$	3.64			(0.3, 0.1, 0.2)	M_3	4.41
		(0.2, 0, 0.4)	$\sim M_1$	3.69		19-25,26	(0.25, 0.25, 0.3)		4.28
	21,22-27	M_1U^x (0.37, 0.1, 0.4)	$\sim M_0$	3.62	4.96	20-28,29	(0.3, 0, 0.25)		4.95
	21-27	(0.3, 0.3, 0.25)	M_0	3.60		20-28	U_1^z-U_1^z (0.5, 0, 0.2)		4.96
	19-25	Z, S_1-S_1 (0.1, 0.1, 0.5)	M_0	3.65		19-33	Σ_2-Σ_1 (0.43, 0.43, 0)		4.94
	20-25	Z, U^x (0.1, 0, 0.5)	M_0	3.60		19-26	Δ_2-Δ_1 (0.18, 0, 0)		4.95
		(0.2, 0.1, 0.3)	$\sim M_0$	3.62		21-29	S_1-S_1 (0.3, 0.3, 0.5)		4.98
	24-28	S_1-S_1 (0.25, 0.25, 0.3)		3.65			U_1^z-U_1^z (0.5, 0, 0.2)		4.96
		T_1-T_1 (0.5, 0.21, 0.5)	M_3	3.74		17-31	Σ_2-Σ_1 (0.42, 0.42, 0)		4.97
	23-28	T (0.5, 0.15, 0.4)	M_1	3.60		23-33	U_1^z-U_1^z (0.5, 0, 0.25)		4.96
	24-27	Δ_1-Δ_2 (0.35, 0, 0)		3.65		22-31	Σ_2-Σ_1 (0.18, 0.18, 0)		4.94

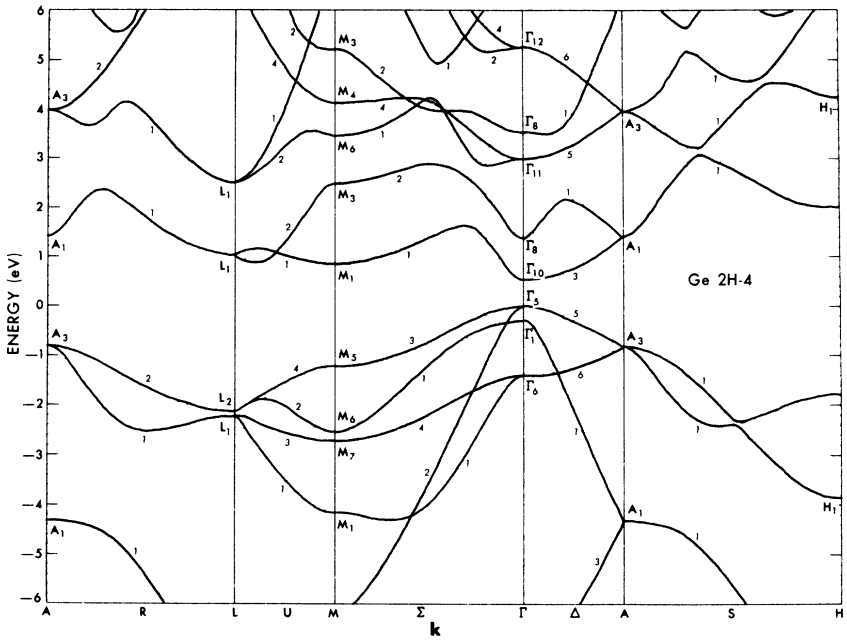

FIG. 2. Band structure of Ge in the $2H$–4 or wurtzite structure.

data are not available at the present, the contributions and identification of strong interband transitions to the optical properties will not vary appreciably with small changes in the form factors.

A. Ge $2H$-4

The threshold in $\epsilon_2^\perp$ (Figs. 2 and 3) at 1.46 eV is caused by Γ_5-Γ_8 transitions and the threshold in $\epsilon_2^\parallel$ at 1.77 eV is caused by Γ_1-Γ_8 transitions. The rise in $\epsilon_2^\perp$ around 2.25 eV is caused by Γ_6-Γ_{10} transitions which are associated with an M_0 critical point (cp) and a region along Δ (Δ_6-Δ_3) with small energy derivatives and large matrix elements. The shoulder at 2.25 eV is caused by an M_1 cp and associated transitions A_3-A_1 at 2.26 eV. The small shoulder near 2.50 eV in $\epsilon_2^\parallel$ seems to be caused by an M_0 cp near the center of the ΓALM face from bands 7-9. However, the shoulder near 2.50 eV in $\epsilon_2^\perp$ is caused by Δ_5-Δ_1 transitions and an M_1 cp approximately $\frac{3}{5}$ of the way from Γ to A. The small peak at 2.68 eV in $\epsilon_2^\perp$ is caused by U_4-U_2 transitions and what seems like an M_1 cp at about $\frac{7}{10}$ of the way from M to L. Although regions off symmetry directions around this critical point also contribute to $\epsilon_2^\parallel$ near 2.68 eV, this effect is overshadowed by U_2-U_2 transitions and an M_1 cp near (0.5, 0, 0.4) at about 2.78 eV. These transitions are responsible for the peak observed around 2.75 eV in $\epsilon_2^\parallel$. The shoulder near 3.15 eV in $\epsilon_2^\parallel$ is caused by 7-10 transitions from a region near the T symmetry direction from an M_0 critical point at about (0.08, 0.08, 0.2) with energy 3.03 eV. In addition 7-9 transitions contribute to this shoulder from a probable M_2 cp at 3.14 eV and near (0.11, 0.11, 0.2). The shoulder in $\epsilon_2^\perp$ at 3.35 eV is caused by transitions from bands 6–9 in a large region mainly in the ΓALM plane around an M_1 cp approximately at (0.2,

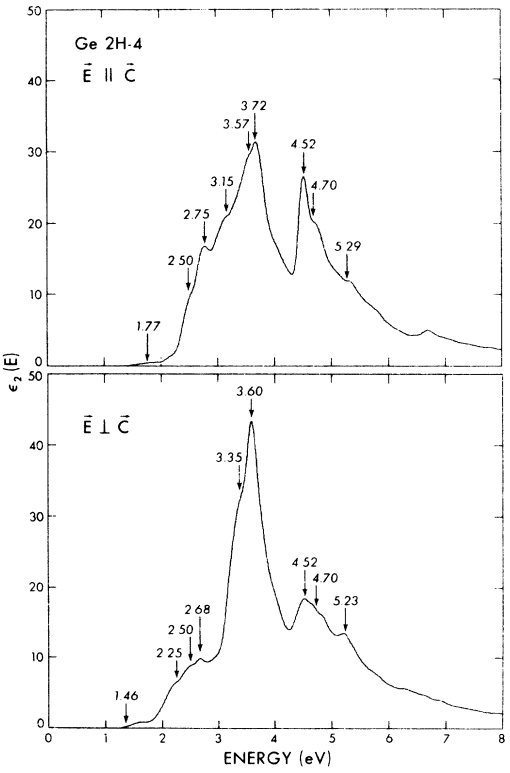

FIG. 3. Imaginary part of the dielectric function, ϵ_2, for Ge $2H$–4 with parallel (top) and perpendicular (bottom) polarizations.

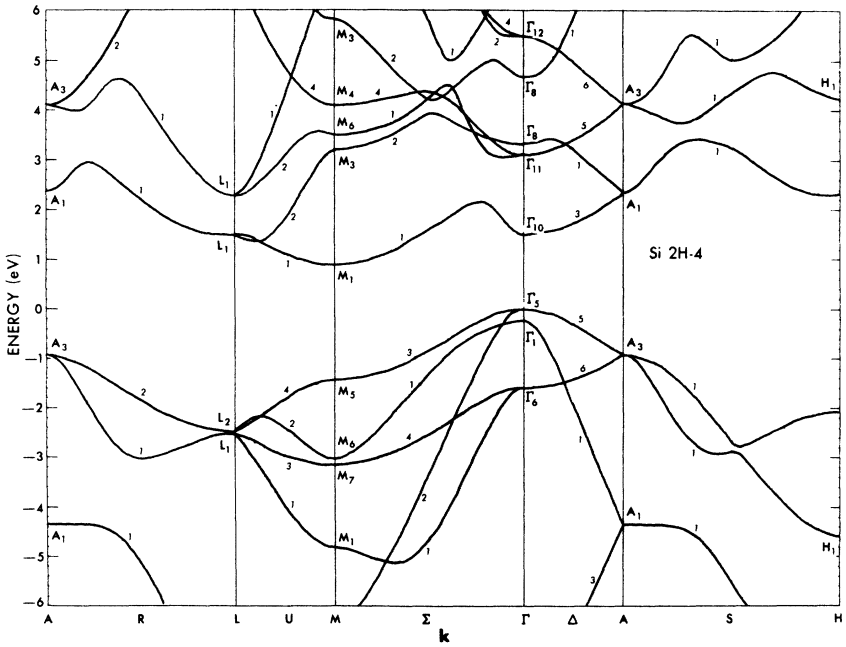

FIG. 4. Band structure of Si in the $2H$–4 or wurtzite structure.

0, 0.25). A similar shoulder in ϵ_2'' at 3.57 eV is caused by a region with large matrix elements around what appears to be an M_1 cp near (0.2, 0.2, 0.35) at about 3.57 eV. The strongest peak in ϵ_2^1 occurs at 3.60 eV and is caused mainly by 6-9 transitions in a large region with strong matrix elements around M_7-M_1 particularly along U_3-U_1 and Σ_4-Σ_1. However, additional strength is obtained by 8-10 transitions in a region around R_2-R_1 about $\frac{1}{2}$ of the way from A to L and from an M_2 cp near (0.2, 0, 0.4) at 3.80 eV. The matrix elements are large for $\hbar\omega < 3.80$ eV and very small for $\hbar\omega > 3.80$ eV. The largest peak in ϵ_2'' occurs at 3.72 eV, caused mainly by an M_1 cp near H at the same energy. The peak in ϵ_2^1 at 4.52 eV is caused by small contributions from three different interband transitions. The main contribution is from 8-11 transitions in a region (U_4-U_2) around L_2-L_1, tentatively designated an M_0 cp at 4.40 eV. A slightly weaker contribution is from bands 8-9, caused by a region around the T symmetry direction with what seems like an M_0 cp near (0.23, 0.23, 0) at 4.45 eV. The final contribution to the peak at 4.52 eV for ϵ_2^1 is probably caused by an M_1 cp near the center of the ΓALM face at 4.53 eV. This critical point provides the strongest contribution to the peak at 4.52 eV for ϵ_2'' because of large matrix elements. The other main contribution to this peak is caused by 8-9 transitions with an M_2 cp at K and a region along T'. The shoulder around 4.70 eV in ϵ_2^1 is mainly caused by 7–9 transitions with a probable M_2 cp at K and a small region extending along T'. Additional contributions to this shoulder are from 8-9 transitions in a small region around (0.4, 0.15, 0.15) with an M_3 cp at 4.72 eV. The final contribution to this shoulder is from a region around A particularly along S with a probable M_2 cp near (0.03, 0.03, 0.45) at

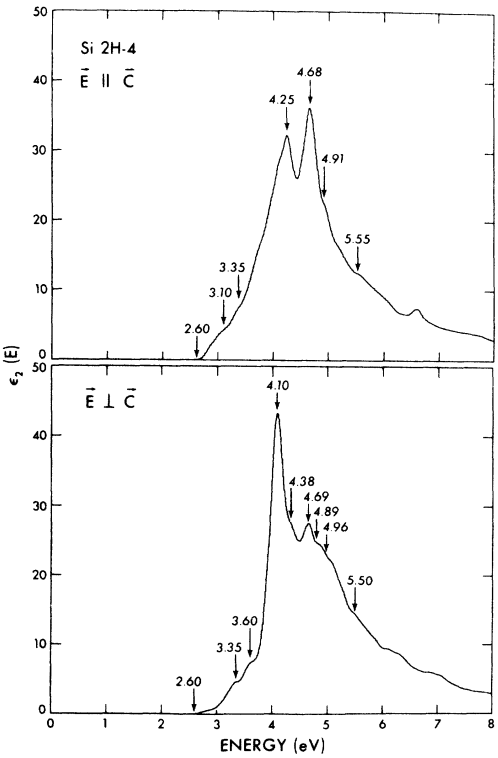

FIG. 5. Imaginary part of the dielectric function, ϵ_2, for Si $2H$–4 with parallel (top) and perpendicular (bottom) polarizations.

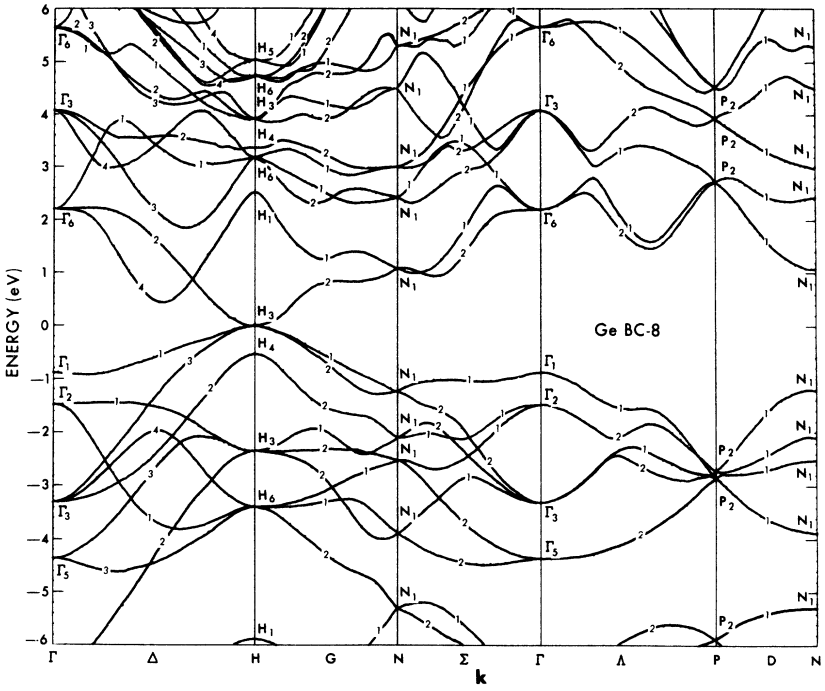

FIG. 6. Band structure of Ge in the BC–8 structure.

4.71 eV. The shoulder in ϵ_2'' around 4.70 eV is caused by an M_0 cp near M about 0.1 of the way along T' and from 7–9 transitions in a region near K along P with a probable M_3 cp at about 4.9 eV near (0.33, 0.33, 0.15). The last discernible peak in $\epsilon_2^\perp$ occurs at 5.23 eV and is caused mainly by Γ_5-Γ_{12} transitions which are associated with an M_2 cp at 5.23 eV. Additional contributions to this peak are from 8-11 transitions in a small region around (0.08, 0.08, 0.35) which has an M_3 cp at 5.30 eV. The last discernible shoulder in ϵ_2'' around 5.29 eV is caused by M_5-M_4 and Σ_3-Σ_4 transitions at 5.33 and 5.31 eV, respectively. We have not determined the symmetry of these critical points. Other contributions to this shoulder are from 8-11 transitions in a small region around (0.3, 0.1, 0.15) at 5.29 eV.

B. Si 2*H*-4

The threshold in $\epsilon_2^\perp$ (Figs. 4 and 5) at 2.60 eV is caused by Σ_1-Σ_1 transitions and a probable M_0 cp near (0.3, 0, 0), while the region around this cp off symmetry directions contributes to the threshold in ϵ_2'' at nearly the same energy. The first shoulder in ϵ_2'' at 3.10 eV is caused by an M_0 cp near the center of the ΓALM face from bands 7-9. The next shoulder in ϵ_2'' occurs around 3.35 eV and is caused by U_2-U_2 transitions with an M_1 cp near (0.05, 0, 0.35) at about 3.34 eV. The rise in $\epsilon_2^\perp$ around 3.35 eV is caused by Γ_6-Γ_{10} transitions which are associated with an M_0 cp and a region along Δ (Δ_6-Δ_3). The shoulder at 3.35 eV is caused by an M_1 cp and associated transitions A_3-A_1. The next shoulder in $\epsilon_2^\perp$ at 3.60 eV is a result of Δ_5-Δ_1 transitions and an M_1 cp approximately $\frac{1}{2}$ of the way from Γ to A. The largest peak in $\epsilon_2^\perp$ at 4.10 eV is caused mainly by 6-9 transitions in a large region with strong matrix elements around M_7-M_1, particularly along U_3-U_1 and Σ_4-Σ_1. To a much lesser extent additional strength to this peak is obtained from a region around R_2-R_1, specifically $\frac{1}{2}$ of the way from A to L. Here we find an M_2 cp near (0.15, 0, 0.5) at about 4.13 eV. The first large peak in ϵ_2'' occurs around 4.25 eV and is caused by a region with large matrix elements around what appears to be an M_1 cp near (0.2, 0.2, 0.35) at about 4.21 eV. In addition a region near H along S', which also has large matrix elements, contributes around 4.26 eV. The shoulder at $\epsilon_2^\perp$ near 4.38 eV is a result of an M_2 cp around (0.2, 0, 0.4) at 4.38 eV and transitions in a region around R_2-R_1 near (0.2, 0, 0.5). The second large peak in ϵ_2'' occurs around 4.68 eV and is the result of several contributions. First we have 8-10 transitions in a region near M about 0.2 of the way along T' where we have a probable M_2 cp at 4.64 eV. Next there are 8-9 transitions in a small region around (0.3, 0.1, 0) with an M_1 cp at 4.68 eV and 7–11 transitions with an M_0 cp at 4.61 eV near (0.4, 0, 0.35). Finally, we have contributions from the shoulder of a nondiscernible peak around 4.75 eV caused by 7-9 transitions along T with what is probably an M_2 cp at 4.74 eV. The peak in $\epsilon_2^\perp$ at 4.69 eV is caused mainly by 8-9 transitions along the T symmetry direction with an M_0 cp at 4.57 eV, and to a lesser extent from Δ_6-Δ_5 transitions with what seems like an M_1 cp at 4.69 eV near (0, 0,

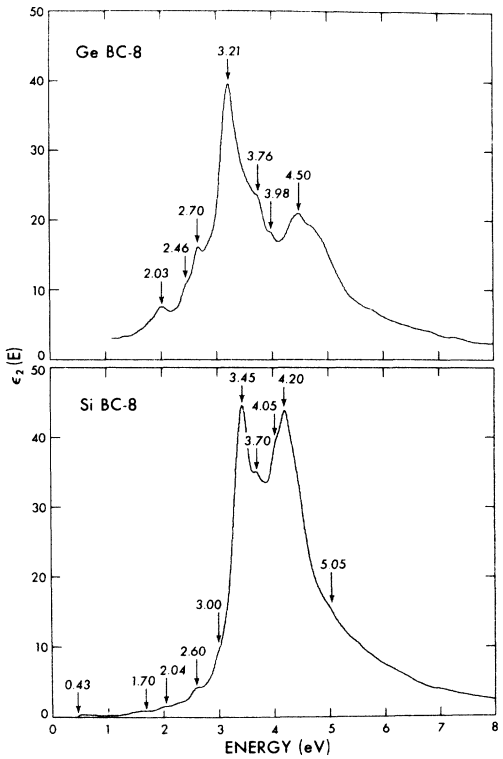

FIG. 7. Imaginary part of the dielectric function, ϵ_2, for Ge BC–8 (top) and Si BC–8 (bottom).

0.3). The peak in $\epsilon_2^{\perp}$ at 4.89 eV is a result of what appears to be an M_2 cp at K around 4.87 eV and a probable M_2 cp near (0.3, 0.25, 0.25) around 4.89 eV. The shoulder in $\epsilon_2^{\parallel}$ at 4.91 eV is caused by a probable M_2 cp for 7-10 and 8-10 transitions at 4.91 and 4.93 eV near (0.2, 0.08, 0) and (0.2, 0.1, 0), respectively. The shoulder in $\epsilon_2^{\perp}$ at 4.96 eV is caused mainly by 8-11 transitions slightly off the Σ direction at a probable M_2 cp near (0.35, 0.05, 0.05) at 4.96 eV, while the shoulder at 5.50 eV is a result of Γ_5-Γ_{12} transitions with an associated M_1 cp at 5.47. Finally the shoulder around 5.55 eV in $\epsilon_2^{\parallel}$ is caused by M_5-M_4 and Σ_3-Σ_4 transitions at 5.61 and 5.54 eV, respectively.

C. Ge BC-8

The first peak in ϵ_2 (Figs. 6 and 7) at 2.03 eV is caused by Σ_1-Σ_2 transitions with an M_1 cp about $\frac{4}{5}$ of the way from Γ to N. The shoulder at 2.46 eV is caused by a small region around Σ_2-Σ_2 with a probable cp near (0.4, 0.4, 0) at 2.46 eV whose symmetry we have not determined. Additional contributions to this shoulder are from Δ_4-Δ_4 transitions and an M_0 cp about $\frac{1}{2}$ the way along Δ at 2.41 eV. The main contribution to the peak at 2.70 eV is from 13-17 transitions in a small region around an M_0 cp near (0.2, 0.8, 0.15) at 2.67 eV. A smaller contribution is from G_2-G_1 transitions with what appears to be on M_0 cp near (0.15, 0.85, 0) at 2.65 eV. The large peak at 3.21 eV is a result of many contributions. First we have 16-19 transitions in a region of large matrix elements around an M_0 cp near (0.25, 0.35, 0.25) at 3.19 eV. Next we have G_1-G_2 transitions with an M_2 cp near (0.4, 0.6, 0) at 3.24 eV and a region of large matrix elements around (0.3, 0.4, 0.15) at about 3.23 eV. Third, there are 14-17 transitions in a region around (0.2, 0.4, 0.15) with what appears to be an M_2 cp at 3.21 eV. Finally, we have 13-18 transitions near (0.3, 0.45, 0) with an M_1 cp at 3.21 eV and G_1-G_1 transitions with a probable cp at (0.22, 0.78, 0) whose symmetry we have not determined. The shoulder around 3.76 eV is also the result of several contributions. The first is from 15-19 transitions in a region near N with G_2-G_1 transitions and an M_3 cp near (0.4, 0.55, 0) at 3.78 eV. Next we have 12-18 transitions near N with G_2-G_1 transitions and an M_1 cp near (0.35, 0.65, 0) at 3.76 eV. Finally, we have contributions from a small region around Γ with Γ_2-Γ_6 transitions and an M_3 cp at 3.74 eV. The shoulder at 3.98 eV is caused by 14-19 transitions in a large region around (0.25, 0.65, 0.15) at 4.0 eV. The last discernible peak occurs at 4.50 eV and is caused by 12-19 transitions in a region around (0.26, 0.63, 0.15) and 14-20 transitions in a large region around (0.1, 0.5, 0.1), both with strong matrix elements. In addition we have contributions from 16-21 transitions in a region around (0.15, 0.2, 0.1) with an M_2 cp near 4.48 eV and Δ_1-Δ_4 transitions with an M_0 cp near (0.25, 0, 0) at 4.42 eV.

D. Si BC-8

The threshold in ϵ_2 (Figs. 7 and 8) at 0.43 eV is caused by H_3-H_4 transitions. The small bump around 1.70 eV is a result of Δ_1-Δ_4 transitions with an M_0 cp near (0.55, 0, 0) at 1.65 eV. The next small bump at 2.04 eV is caused by what appears to be an M_2 cp near (0.3, 0.55, 0). The shoulder at 2.60 eV is primarily caused by Σ_1-Σ_2 transitions with an M_2 cp near (0.4, 0.4, 0) at 2.62 eV. Additional structure is obtained by 15-17 transitions in a region around an M_0 cp near (0.3, 0.5, 0) at 2.54 eV. The shoulder at 3.0 eV is caused by 13-17 transitions in a small region around an M_0 cp near (0.2, 0.7, 0.15) at 2.96 eV. The large peak at 3.45 eV is the result of many contributions. The first is from 13-17 transitions in a region of very large matrix elements around (0.1, 0.5, 0.1) at about 3.46 eV. Next we have 14-17 transitions in a region around what appears to be an M_2 cp near (0.2, 0.4, 0.15) at 3.45 eV with strong matrix elements. Also, there are 16-19 transitions in a small region with very large matrix elements and an M_1 cp near (0.3, 0.4, 0.2) at 3.43 eV. Finally there is a region around Γ_1-Γ_6 transitions with an associated M_0

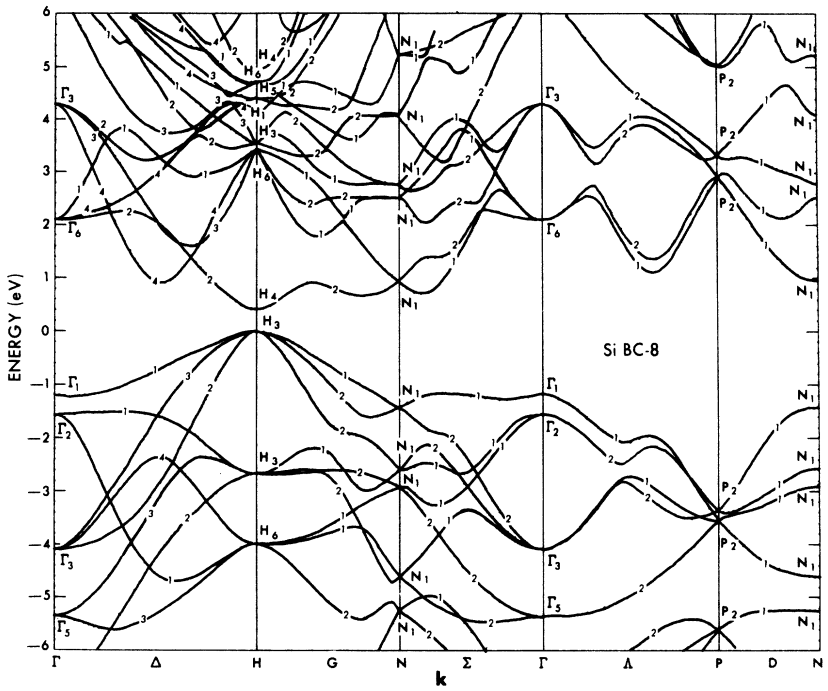

FIG. 8. Band structure of Si in the BC–8 structure.

cp at 3.38 eV. The shoulder at 3.7 eV is caused by a small region around G_1-G_2 transitions with an M_2 cp at 3.7 eV near (0.45, 0.55, 0) and by a small region around D_1-D_1 transitions with large matrix elements and an M_1 cp at 3.68 eV around (0.5, 0.5, 0.15). The shoulder at 4.05 eV is the result of several types of transitions. First we have 16-21 transitions in a small region around (0.2, 0.6, 0.15) with large matrix elements and Δ_1-Δ_2 transitions with an M_2 cp near (0, 5, 0, 0) at 4.04 eV. Next we have 15-21 transitions in a small region around (0.2, 0.6, 0.1) with an associated M_0 cp at 4.02 eV and G_1-G_1 (13-18) transitions with a probable cp near (0.2, 0.8, 0) whose symmetry we have not yet determined. Finally we have 14-19 transitions in a region around what appears to be an M_1 cp near (0.25, 0.65, 0.1) at 4.07 eV. The large peak at 4.20 eV is mainly caused by 16-22 transi-

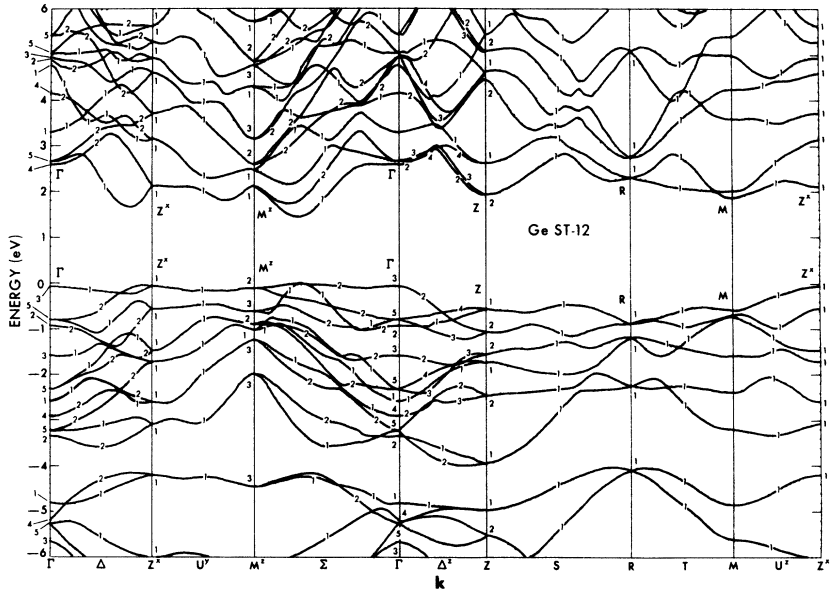

FIG. 9. Band structure of Ge in the ST–12 structure.

tions in a region of very large matrix elements around what appears to be an M_2 cp near (0.2, 0.5, 0) at 4.20 eV. In addition we have contributions from 12-18 and 15-22 transitions in a small region around an M_2 cp near (0.15, 0.7, 0.15) at 4.22 eV and an M_0 cp near (0.15, 0.7, 0) at 4.14 eV, respectively. Finally, the shoulder at 5.05 eV can be attributed to 14-21 transitions in a small region around an M_2 cp near (0.2, 0.6, 0.1) at 5.05 eV and D_1-D_1 transitions with a probable cp near (0.5, 0.5, 0.1) at 5.0 eV whose symmetry we have not determined.

E. Ge ST-12

In this section and the section on Si ST-12 we shall treat the perpendicular component of $\epsilon_2^{\perp}$ first and discuss the parallel component in the last paragraph.

The threshold in $\epsilon_2^{\perp}$ (Figs. 9 and 10) occurs at 1.46 eV and is caused by Σ_1-Σ_1 transitions. The shoulder at 2.10 eV is caused by equal contributions from 24-25 and 23-25 transitions in small regions (tubular along the z direction) around an M_0 cp near (0.4, 0.1, 0.3) at 2.08 eV and an M_1 cp near (0.4, 0, 0.3) at 2.18 eV, respectively. The shoulder around 2.55 eV is caused mainly by 24-26 transitions in a region around an M_1 cp near (0.5, 0.1, 0.3) at 2.48 eV along with much weaker contributions from T_1-T_1 (0.5, 0.5, 0.4) and U_1^z-U_1^z (0.5, 0, 0.3) transitions at 2.52 and 2.50 eV, respectively, whose critical-point symmetries have not been determined. Next we have 23-26 transitions in a region of relatively large matrix elements around (0.4, 0.15, 0.25) contributing at 2.62 eV. Other contributions to this shoulder are from 22-25 and 21-25 transitions, with a probable M_2 cp near (0.4, 0, 0.25) at 2.62 eV and an M_1 cp near (0.4, 0.15, 0.25) at 2.60 eV, respectively, along with transitions at M in a much weaker sense at 2.60 eV. Finally, we have 24-25 transitions with an M_0 cp near (0.1, 0.1, 0.4) at 2.54 eV.

The peak around 2.80 eV is the result of several types of transitions whose contributions are all of comparable weight. First we have 23, 24-26 transitions in a region (mostly along the z direction) around S_1-S_1 with an M_2 cp near (0.4, 0.4, 0.5) at 2.87 eV. Next there are 21-25 transitions in a region around an M_1 cp near (0.4, 0.15, 0.25) at 2.60 eV which contributes to 2.75 eV because of matrix elements, and in a weaker sense Δ_1-Δ_1 (0.4, 0, 0) transitions with a cp of undetermined symmetry at 2.80 eV. Next we have 24-25 transitions near the U^x symmetry direction with an M_1 cp near (0.2, 0, 0.4) at 2.70 eV. Finally, we have 24-27 transitions in a small region (tubular along the z direction) around an M_1 cp near (0.5, 0.1, 0.3) at 2.76 eV, along with some weaker Γ_3-Γ_5 transitions with an M_0 cp at 2.75 eV. The shoulder around 3.0 eV is caused mainly by 20-25 transitions in a region (tubular along the z direction) around an M_0 cp near (0.4, 0.15, 0.25) at 2.93 eV and 22-25 transitions in a region around Z_2-Z_2 with an associated M_0 cp at 2.98 eV along with much weaker T_1-T_1 (0.5, 0.5, 0.3) transitions at 3.0 eV. Additional contributions to this shoulder are from 24-27 transitions in a small region near R along T^z with an M_1 cp near (0.5, 0.5, 0.45) at 3.11 eV and 19-25 transitions in a region of relatively large matrix elements around (0.35, 0.18, 0) at 2.97 eV, along with weaker M_2^z-M_1^z transitions with what appears to be an M_2 cp at 3.0 eV. Finally, we have 22-27 transitions with an M_0 cp near (0.5, 0.15, 0.3) at 3.04 eV.

The next shoulder around 3.20 eV is caused mainly by Z_1-Z_1 transitions with an associated M_0 cp at 3.18 eV along with much weaker transitions Z_1^x-Z_1^x with an M_3 cp at 3.20 eV. Other contributions to this peak are from 21-25 transitions in a small region around U^x with an M_2 cp near (0.2, 0, 0.5) at 3.21 eV and 23-28 transitions in a region (tubular along z direction) near R mostly along T^z with a probable M_1 cp at 3.20 eV. Finally, we also have contributions from 19-25 transitions with an M_2 cp near (0.5, 0.15, 0.3) at 3.21 eV, along with weaker Δ_1-Δ_1 transitions near (0.38, 0, 0) at 3.20 eV. The peak at 3.50 eV is caused mainly by 19-

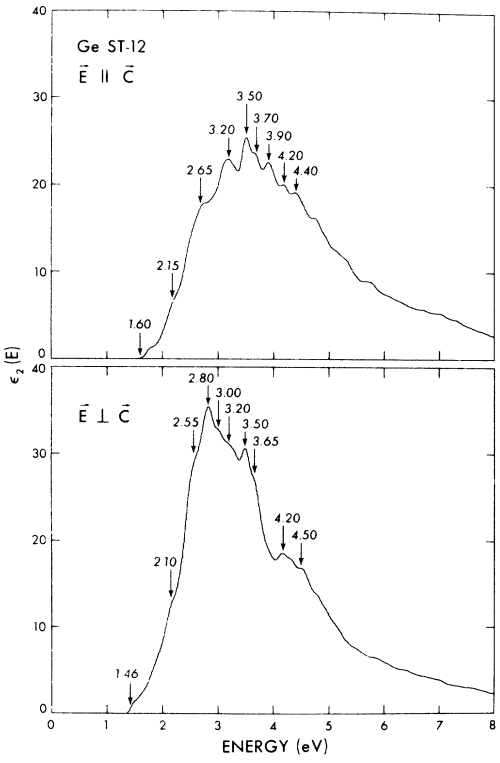

FIG. 10. Imaginary part of the dielectric function, ϵ_2, for Ge ST-12 with parallel (top) and perpendicular (bottom) polarizations.

25, 26 transitions in a region (along the z direction) around R_1-R_1 with an M_0 cp at 3.46 eV, and 18-25 transitions in a small region around T_1-T_1 near (0.5, 0.22, 0.5) with a probable M_0 cp at 3.49 eV. Additional contributions are from S_1-S_1 (20-25) transitions with an M_0 cp near (0.06, 0.06, 0.5) at 3.45 eV and what appears to be an M_1 cp near (0.45, 0.45, 0.5) also at 3.45 eV. Other contributions are from 17-25 transitions in a small region along T^z near (0.5, 0.5, 0.3) with a probable M_1 cp at 3.53 eV and 24-27 transitions with a probable M_2 cp near 0, 0.1, 0.25) at 3.47 eV, and to a lesser extent T_1-T_1 transitions near (0.5, 0.3, 0.5) at about 3.50 eV. Finally, we have T_1-T_1 (20-26) transitions with an M_2 cp at 3.47 eV and 22-27 transitions with an M_2 cp near 3.54 eV, and to a lesser extent Δ_1-Δ_1 transitions near (0.45, 0, 0) contributing at 3.50 eV.

The shoulder at 3.65 eV is caused by 17-25 transitions in a region (tubular along the z direction) around an M_2 cp at 3.67 eV near (0.5, 0.25, 0.3), and in a weaker sense by Z_1-Z_2 transitions with an M_0 cp at 3.65 eV. Other contributions to this shoulder are from 23-27 transitions in a relatively large region around (0.1, 0, 0.25) which contributes around 3.65 eV, 24-29 transitions in a region around U^x with an M_0 cp near (0.22, 0, 0.5) at 3.60 eV, and 24-30 transitions at R with an M_1 cp at 3.60 eV. The peak at 4.20 eV is caused by 24-30 transitions in a region (mostly in the z direction) near U^x around (0.3, 0, 0.4) which contributes at about 4.18 eV, along with weaker transitions in a region around M at 4.20 eV. In addition we have 21-27 transitions with an M_2 cp near (0.15, 0.15, 0.2) at 4.22 eV and 23-28 transitions in a region around Δ_2-Δ_1 with most of the contributions near (0.1, 0, 0.05) at 4.20 eV. Other transitions contributing to this peak are 21-28 transitions in a small region near U^x around (0.15, 0, 0.4) at 4.20 eV and 20-25 transitions around Σ_2-Σ_1 with an M_1 cp near (0.07, 0.07, 0) at 4.21 eV. Finally, we also have some weak structure from S_1-S_1 (23-32) transitions with a cp of undetermined symmetry near (0.22, 0.22, 0.5) at 4.20 eV.

The last peak that we shall consider in $\epsilon_2^{\perp}$ occurs at 4.50 eV and is the result of many different contributions. First we have 23-31 transitions in a region around U_1^z-U_1^z with a probable M_3 cp near (0.5, 0, 0.2) at 4.57 eV and Σ_2-Σ_1 (21-23) transitions with a cp of undetermined symmetry near (0.4, 0.4, 0) at 4.48 eV. Next we have 22-30 transitions in a small region near U^y with an M_1 cp around (0.45, 0.1, 0.05) at 4.36 eV and an M_1 cp near (0.3, 0.15, 0.4) at 4.52 eV. In addition we have 20-26 transitions with an M_3 cp near (0.15, 0, 0.1) at 4.54 eV and 20-28 transitions with an M_0 cp near (0.15, 0.15, 0.25) at 4.47 eV. Finally for completeness we also list in Table III a set of much weaker transitions along symmetry directions at critical points of undetermined symmetry, starting with M_3^z-M_1^z transitions and ending with U_1^y-U_1^y transitions. Taken as a whole they are of comparable weight to the others discussed above.

The threshold in $\epsilon_2^{\parallel}$ occurs around 1.60 eV with minute matrix elements from Σ_2-Σ_1 transitions at 1.46 eV and very small matrix elements near 1.6 eV, and appreciable contributions only from Δ_2-Δ_1 transitions with a probable M_1 cp near (0.4, 0, 0) at 1.7 eV. The shoulder around 2.15 eV is caused mainly by Σ_2-Σ_1 transitions with an M_0 cp near (0.37, 0.37, 0) at 2.07 eV. In addition we have contributions from 24-25 and 23-25 transitions in small regions around what appears to be an M_0 cp near (0.4, 0.1, 0.3) at 2.08 eV and an M_1 cp near (0.4, 0, 0.3) at 2.18 eV, respectively. The shoulder around 2.65 eV is caused mainly by 21-15 transitions in a region around an M_1 cp near (0.4, 0.15, 0.25) at 2.60 eV and a region (particularly along U^y) around Z_1^x-Z_1^x with a probable M_2 cp at 2.65 eV, and U_1^y-U_1^y transitions contributing at 2.63 eV. Additional contributions are from 22-26 transitions with an M_1 cp near (0.5, 0.2, 0.25) at 2.74 eV and 22-25 transitions in a region around M_3^z-M_1^z with a probable M_2 cp at 2.70 eV. Finally, to a much lesser extent, we have contributions from Γ_3-Γ_4 transitions with an M_0 cp at 2.64 eV.

The peak at 3.20 eV is a result of several interband contributions of approximately the same weight. First we have 24-27 transitions in a region around Z_1-Z_1 with an M_0 cp at 3.18 eV, along with weaker Z_1^x-Z_1^x transitions with an M_3 cp at 3.20 eV and Δ_2-Δ_1 transitions with a probable M_2 cp near (0.45, 0, 0) at 3.18 eV. Next we have 21-25 transitions in a small region (mostly along the z direction) around U^x with an M_2 cp near (0.2, 0, 0.5) at 3.21 eV and a region of large matrix elements near (0.2, 0.2, 0.3) contributing to 3.20 eV. In addition we have 24-26 transitions in a region around S_1-S_1 with an M_3 cp near (0.26, 0.26, 0.5) at 3.26 eV, and in a weaker sense R_1-R_1 (23-28) transitions at 3.20 eV and Σ_2-Σ_1 (24-28) transitions with a probable M_1 cp near (0.25, 0.25, 0) at 3.20 eV. The next peak at 3.50 eV is a result, in part, of 20-25 transitions in a region around Z_2-Z_2 with a cp of undetermined symmetry at 3.48 eV and S_1-S_1 transitions with an M_0 cp near (0.06, 0.06, 0.5) at 3.45 eV. In addition there are contributions from 22-27 transitions in a small region around an M_2 cp near (0.3, 0.1, 0.3) at 3.54 eV, Γ_5-Γ_5 transitions with an associated M_0 cp at 3.44 eV, and 20-26 transitions in a region (tubular along the z direction) of relatively large matrix elements around (0.3, 0.1, 0.3) at 3.53 eV. Finally, there are weaker contributions from Σ_2-Σ_1 (24-29) and Δ_1-Δ_2 (24-26) transitions with critical points of undetermined symmetry near (0.35, 0.35, 0) at 3.45 eV and near

(0.3, 0, 0) at 3.48 eV, respectively.

The shoulder at 3.70 eV is caused by 24-28 transitions in a small region around Δ_1-Δ_2 with a cp of undetermined symmetry near (0.26, 0, 0) at 3.70 eV and S_1-S_1 transitions with a probable M_2 cp near (0.2, 0, 0) also at 3.70 eV. Other contributions to this shoulder are from 21-27 transitions around Z_1^x-Z_1^x with an M_1 cp at 3.69 eV and U_1^z-U_1^z transitions with a cp of undetermined symmetry near (0.5, 0, 0.2) at 3.71 eV. The peak at 3.90 eV is caused in part by 19-25 transitions in a small region (mostly in the z direction) around an M_3 cp near (0.2, 0.15, 0.3) at 3.92 eV and 24-29 transitions around Δ_2^z-Δ_2^z with an M_2 cp near (0, 0, 0.18) at 3.94 eV. Additional contributions are from 23-29 transitions around Δ_1-Δ_2 with what appears to be an M_2 cp at 3.9 eV, S_1-S_1 transitions with a cp of undetermined symmetry at 3.9 eV, and Δ_2-Δ_1 (21-26) transitions with a probable M_1 cp near (0.15, 0, 0) at 3.88 eV. The peak at 4.20 eV is caused in part by 24-29 transitions in a region of very large matrix elements around Γ_3-Γ_4 with an M_3 cp at 4.22 eV and 20-25 transitions in a region around Γ_3-Γ_4 with an M_0 cp at 4.16 eV, along with an M_1 cp near (0.07, 0.07, 0) at 4.21 eV from Σ_2-Σ_1 transitions. Other contributions to this peak are from 21-28 transitions in a region around Γ_2-Γ_1 with an M_0 cp at 4.22 eV, including in particular Δ_1^z-Δ_1^z transitions at 4.23 eV, transitions in a small region near U^x around (0.15, 0, 0.4) at 4.20 eV, and to a lesser extent S_1-S_1 transitions with a cp of undetermined symmetry at 4.20 eV. Still other contributions are from 22-29 transitions with an M_0 cp near (0.15, 0.15, 0.2) at 4.21 eV and weaker Z_1^x-Z_1^x transitions with an M_2 cp at 4.24 eV. Finally, we have 24-30 transitions with an M_1 cp near (0.1, 0.1, 0.3) at 4.26 eV and 22-30 transitions in a region around (0.3, 0.25, 0.25) contributing at 4.21 eV.

The last peak that we shall consider in $\epsilon_2^{\parallel}$ occurs at 4.40 eV and is the result of many different contributions. First we have 20-26 transitions in a region (tubular along the z direction) around an M_2 cp near (0.17, 0.17, 0.1) at 4.42 eV and 18-27 transitions in a region around Z_1-Z_1 with an M_0 cp at 4.36 eV. Next we have 23-28 (Σ_1-Σ_2) transitions and 22-27 (Σ_1-Σ_2) transitions with critical points of undetermined symmetry near (0.14, 0.14, 0) at 4.40 and 4.37 eV, respectively, along with Δ_1-Δ_2 transitions with a cp near (0.25, 0, 0) at 4.40 eV. Other contributions are from 23-24 transitions around M_2^z-M_1^z, with a probable M_2 cp at 4.40 eV and Σ_1-Σ_2 transitions with a cp of undetermined symmetry near (0.35, 0.35, 0) at 4.40 eV. In addition we have weaker contributions from 16-26 transitions in a small region around Z_2-Z_2, particularly along Δ_2^z-Δ_3^z at 4.40 eV, with a probable M_1 cp at 4.37 eV. Finally we have 23-30 transitions with an M_3 cp near (0.35, 0.15, 0.3) at 4.42 eV, Δ_1-Δ_2 transitions with a cp of undetermined symmetry near (0.37, 0, 0) at 4.40 eV, and 22-31 transitions around U_1^y-U_1^y with a cp near (0.5, 0.3, 0) at 4.40 eV.

F. Si ST-12

The threshold in $\epsilon_2^{\perp}$ (Figs. 11 and 12) occurs at 1.76 eV and is the result of 24-25 transitions around an M_0 cp near (0.4, 0.2, 0). The shoulder at 2.33 eV is caused by 23-25 transitions and 24-25 transitions in a region (tubular along the z direction) around an M_0 cp near (0.4, 0, 0.3) at 2.31 eV and around an M_1 cp near (0.4, 0, 0.45) at 2.33 eV,

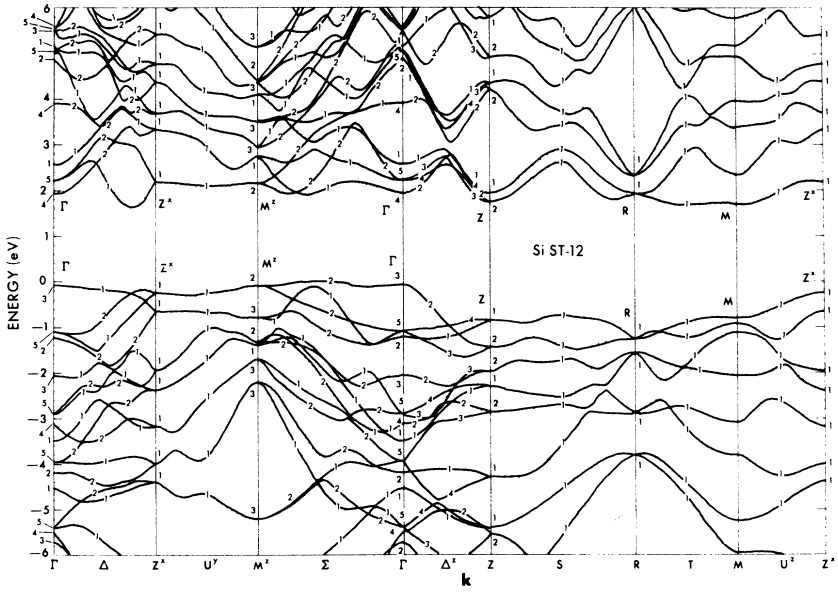

FIG. 11. Band structure of Si in the ST–12 structure.

respectively. The shoulder at 2.50 eV is caused by 23-26 and mainly 24-26 transitions in a region around M with a probable M_1 cp at 2.50 eV. In particular, we have contributions from T_1-T_1 transitions with an M_1 cp near (0.5, 0.15, 0.5) at 2.52 eV and U_1^z-U_1^z transitions at 2.51 eV. Finally, we have weaker transitions from a region near Z^x along U_1^y-U_1^y contributing to 2.45 eV.

The peak at 2.80 eV is a result in part of 23, 24-26 transitions in a region around S_1-S_1 (0.4, 0.4, 0.5) at 2.76 eV, with particularly strong contributions off the symmetry axis with an M_1 cp near (0.4, 0.4, 0.4) at 2.80 eV. Other contributions are from 21-25 transitions with an M_0 cp near (0.45, 0.15, 0.3) at 2.73 eV, Δ_2-Δ_1 transitions with a cp of undetermined symmetry near (0.45, 0, 0) at 2.80 eV, and U_1^y-U_1^y transitions with an M_1 cp near (0.5, 0.2, 0) at 2.79 eV, along with 22-26 transitions in a large region (along the z direction) around (0.5, 0.3, 0.15) contributing at 2.82 eV. Finally, we have contributions from Z_1-Z_1 (23-28) transitions with an M_0 cp at 2.78 eV and 22-25 transitions with an M_2 cp near (0.4, 0, 0.25) at 2.74 eV. The shoulder at 3.20 eV is caused mostly by 20-25 transitions in a region of relatively large matrix elements around Δ_1-Δ_1, with an M_0 cp near (0.39, 0, 0) at 3.17 eV and a region around Σ_1-Σ_1 with an M_2 cp near (0.37, 0.37, 0) at 3.21 eV, along with 19-25 transitions in a region (along the z direction) around Σ_1-Σ_2 with a probable M_1 cp near (0.4, 0.4, 0) at 3.18 eV. Additional contributions are from 22-25 transitions in a region around Z_2-Z_2 with an M_0 cp at 3.18 eV and an M_1 cp near (0.2, 0.2, 0.25) at 3.16 eV, and 20-26 transitions in a region around U^y with an M_1 cp near (0.5, 0.35, 0.05) at 3.17 eV and a cp of undetermined symmetry near (0.4, 0.4, 0) from Σ_1-Σ_1 transitions at 3.20 eV. Other contributions are from 22-28 transitions, from a cp of undetermined symmetry around U_1^y-U_1^y near (0.5, 0.4, 0) at 3.20 eV, and R_1-R_1 transitions at 3.20 eV, and 21-26 transitions in a region around T^z with an M_2 cp near (0.5, 0.5, 0.4) at 3.23 eV.

The largest peak in $\epsilon_2^\perp$ occurs at 3.38 eV and is the result of many types of transitions. First we have 20-25 transitions in a region near R along T^z with an M_1 cp near (0.5, 0.5, 0.45) at 3.39 eV and 19-25 transitions in a similar region around T^z with a probable M_3 cp near (0.48, 0.48, 0.4) at 3.45 eV, along with Σ_2-Σ_1 transitions near (0.35, 0.35, 0) with a cp of undetermined symmetry at 3.35 eV. Next we have 22-26 transitions with a large region (along the z direction) around an M_2 cp near (0.25, 0.25, 0.3) at 3.36 eV. Additional contributions are from 18-25 transitions with an M_0 cp near (0.4, 0.2, 0) at 3.35 eV, U_1^y-U_1^y transitions near (0.5, 0.38, 0) with a cp at 3.4 eV, 24-27 transitions with an M_1 cp near (0.15, 0, 0.3) at 3.38 eV, and U_1^z-U_1^z transitions near (0.5, 0, 0.15) with a cp around 3.38 eV. Finally we have 22-28 transitions with an M_0 cp at 3.37 eV from Z_2-Z_1 transitions and an M_1 cp near (0.45, 0.4, 0.3) at 3.35 eV, and 23-27 transitions with contributions from various regions of the zone contributing at around 3.35 eV. The shoulder at 3.60 eV is caused in part by 20-25 transitions in a region near Z around U^x with an M_0 cp near (0.1, 0, 0.5) at 3.60 eV and 21-26 transitions with a probable M_1 cp near (0.3, 0.2, 0.25) also at 3.60 eV. Other contributions are from 22-27 transitions in a region around Σ_2-Σ_1 with an M_0 cp near (0.3, 0.3, 0) at 3.50 eV, 21-29 transitions in a region around R_1-R_1 with an M_0 cp at 3.59 eV, and 23-27 transitions with an M_0 cp near (0.1, 0.1, 0.25) at 3.54 eV. Finally we have 23-28 transitions with an M_1 cp near (0.5, 0.15, 0.3) at 3.58 eV, 22-26 transitions in a region around Δ_2^z-Δ_4^z with a cp of undetermined symmetry near (0, 0, 0.3) at 3.60 eV, and 22-28 transitions in a region around Σ_2-Σ_1 with a cp near (0.32, 0.32, 0) at 3.60 eV.

The peak around 3.85 eV is the result of many types of transitions contributing approximately equally to $\epsilon_2^\perp$. First we have 24-29 transitions in a region around Z_1^x-Z_1^x with an M_2 cp at 3.92 eV and 23-28 transitions in a region (tubular along the z direction) around Γ_5-Γ_1 with an M_0 cp at 3.71 eV

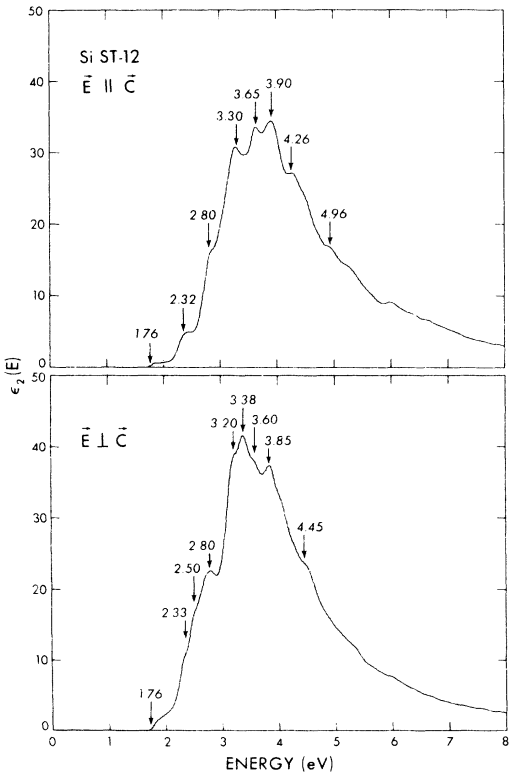

FIG. 12. Imaginary part of the dielectric function, ϵ_2, for Si ST–12 with parallel (top) and perpendicular (bottom) polarizations.

along with Δ_4^z-Δ_1^z transitions with an M_2 cp near (0, 0, 0.24) at 3.85 eV. Next we have 23-29 transitions in various regions of the zone with strongest contributions from a large tubular region in the z direction around (0.35, 0.15, 0.25) contributing at 3.85 eV and 17-25 transitions in a large region around U_1^z-U_1^z (0.5, 0, 0.33) parallel to the T direction contributing at 3.85 eV. Other contributions are from 22-27 transitions, with a probable M_1 cp near (0.15, 0.15, 0.2) at 3.81 eV, 21-29 transitions with contributions from a small region around Σ_1-Σ_2 and an M_1 cp near (0.42, 0.42, 0) at 3.88 eV, and 20-26 transitions with what appears to be an M_1 cp near (0.15, 0.1, 0.4) at 3.89 eV. Finally, we have 16-25 transitions in a region around M_3^z-M_2^z with an M_1 cp at 3.86 eV and 23-20 transitions with a probable M_1 cp near (0.35, 0.35, 0.25) at 3.81 eV.

The last structure we shall consider in the $\epsilon_2^\perp$ spectrum occurs at 4.45 eV. This shoulder is caused in part by 20-26 transitions in a region (along the z direction) around what appears to be an M_2 cp near (0.1, 0, 0.1) at 4.48 eV, Σ_1-Σ_1 transitions with a cp of undetermined symmetry near (0.12, 0.12, 0) at 4.44 eV, and 23-25 transitions with a cp at M_2^z-M_3^z at 4.46 eV. Other contributions are from 15-27 transitions in a region around M_3^z-M_1^z with a probable M_1 cp at 4.45 eV and 15-26 transitions near M^z with a cp from Σ_2-Σ_1 transitions near (0.44, 0.44, 0) at 4.42 eV along with U_1^z-U_1^z transitions with a cp near (0.5, 0, 0.34) at 4.45 eV. Next we have 14-26 transitions with a cp at M_3^z-M_2^z at 4.41 eV and a cp from T_1-T_1 transitions near (0.5, 0.28, 0.5) at 4.45 eV, and 21-27 transitions with a probable M_1 cp near (0.2, 0, 0.2) at 4.40 eV and a cp from Δ_3^z-Δ_2^z transitions near (0, 0, 0.27) at 4.45 eV. Finally we have contributions from Σ_2-Σ_1 (22-33) transitions with a cp near (0.44, 0.44, 0) at 4.45 eV, Σ_1-Σ_1 (22-33) transitions with a cp near (0.4, 0.4, 0) at 4.45 eV, 19-27 transitions with an M_2 cp near (0.35, 0.15, 0.3) at 4.48 eV, and a series of weaker transitions listed for completeness in Table V.

The threshold in $\epsilon_2^\parallel$ occurs at 1.76 eV and is the result of 24-25 transitions around an M_0 cp near (0.4, 0.2, 0) which are weaker than in the $\epsilon_2^\perp$ case. The shoulder starting at 2.32 eV is caused in part by 23-25 transitions and 24-25 transitions in a region (mostly along the z direction) around an M_0 cp near (0.4, 0, 0.3) at 2.31 eV and around an M_1 cp near (0.4, 0, 0.45) at 2.33 eV, respectively. Other contributions are from 24-26 transitions in a region around U_1^z-U_1^z with an M_0 cp near (0.5, 0, 0.4) at 2.46 eV and 22-25 transitions in a region around Σ_2-Σ_1 with an M_0 cp near (0.35, 0.35, 0) at 2.32 eV. The shoulder around 2.80 eV is caused to a large extent by 24-26 transitions in a small region around an M_0 cp near (0.1, 0.1, 0.4) at 2.81 eV and an M_0 cp near (0.2, 0.2, 0.5) at 2.79 eV. Other strong contributions are from 21-25 transitions with an M_0 cp near (0.45, 0.15, 0.3) at 2.73 eV, U_1^y-U_1^y transitions with an M_1 cp near (0.5, 0.2, 0) at 2.78 eV, and 22-26 transitions in a region (along the z direction) around (0.5, 0.3, 0.15) at 2.82 eV and an M_0 cp at M at about 2.65 eV. Weaker contributions are from Z_1-Z_1 (24-27) transitions with an M_0 cp at 2.79 eV and 24-25 transitions with an M_2 cp near (0.2, 0.05, 0.4) at 2.81 eV.

The peak at 3.30 eV is caused in part by 21-25 transitions in a region (tubular along the z direction) around U^x with an M_2 cp near (0.2, 0, 0.5) at 3.33 eV and 23-27 transitions with an M_1 cp near (0.35, 0.15, 0.3) at 3.31 eV. Additional contributions to this peak are from 22-26 transitions in a region around what appears to be an M_2 cp near (0.25, 0.25, 0.3) at 3.36 eV and 23-26 transitions in a region near Γ, with particularly strong contributions from Δ_4^z-Δ_4^z transitions at about 3.3 eV. Finally we have contributions from 24-26 transitions with an M_2 cp near (0.12, 0.12, 0.25) at 3.25 eV and 21-28 transitions in a region around Σ_2-Σ_1 with a cp of undetermined symmetry near (0.4, 0.4, 0) at 3.3 eV. The peak at 3.65 eV is the result of three main types of contributions. First, we have 22-27 transitions in a region near Z off the S direction with a probable M_1 cp near (0.15, 0.1, 0.45) at 3.64 eV, along with an M_1 cp near (0.2, 0, 0.4) at 3.69 eV, and 21, 22-27 transitions in a region of relatively large matrix elements near M off the U^x direction with a probable M_0 cp near (0.37, 0.1, 0.4) at 3.62 eV and an M_0 cp near (0.3, 0.3, 0.25) at 3.60 eV. Second, we have 19-25 transitions, in a region near Z around S_1-S_1, with an M_0 cp near (0.1, 0.1, 0.5) at 3.65 eV and 20-25 transitions also near Z, but around U^x with an M_0 cp near (0.1, 0, 0.5) at 3.60 eV and what appears to be an M_0 cp near (0.2, 0.1, 0.3) at 3.62 eV. Third, we have 24-28 transitions with a cp of undetermined symmetry near S_1-S_1 (0.25, 0.25, 0.5) at 3.65 eV and a region around T_1-T_1 with an M_3 cp near (0.5, 0.21, 0.5) at 3.74 eV, and 23-28 transitions with an M_1 cp near T at about (0.5, 0.15, 0.4) at 3.60 eV, along with weaker Δ_1-Δ_2 (24-27) transitions with a cp near (0.35, 0, 0) at 3.65 eV.

The large peak at 3.90 eV is caused in part by 24-30 transitions in a region around an M_1 cp near (0.5, 0.22, 0.25) at 3.92 eV and 24-29, 30 transitions in a region around Z_1^x-Z_1^x with an M_0 cp at 3.93 eV, and particularly strong contributions along U_1^y-U_1^y at 3.95 eV. Other important contributions are from 24-29 transitions in a region with very large matrix elements around Γ_3-Γ_4 with an M_2 cp at 3.98 eV and 23-29 transitions with an M_0 cp near (0.2, 0, 0.3) at 3.91 eV. Next we have 18-25 transitions in a region around (0.3, 0, 0.4) contributing at 3.90 eV, Δ_2-Δ_1 transitions with a cp near (0.35, 0, 0) also at 3.90 eV, and 21-26 transitions in a region

around Σ_2-Σ_1 with an M_1 cp near (0.16, 0.16, 0) at 3.92 eV. Finally we have 22-30 transitions with an M_0 cp near (0.35, 0.35, 0.1) at 3.81 eV and 23-28 transitions with a cp near (0, 0, 0.22) at 3.88 eV.

The shoulder around 4.26 eV is caused in part by 20-25 transitions in a region (along the z direction) of large matrix elements around Γ_3-Γ_4 with an M_0 cp at 4.07 eV, 22-29 transitions in a region (along the z direction) around M with a probable M_1 cp at 4.28 eV, and 22-32 transitions in a region around M_3^z-M_3^z with a cp at 4.30 eV and in a region around U_1^y-U_1^y with a cp near (0.5, 0.3, 0) at 4.26 eV. Additional contributions to this shoulder are from 20-28 transitions in a region around (0.4, 0.2, 0.25) at 4.30 eV, 18-27 transitions in a region around Z_1-Z_1 with an M_1 cp at 4.25 eV, and 19-25, 26 transitions in a region around (0.25, 0.25, 0.3) at 4.28 eV. Finally, we have 24-30 transitions with critical points of undetermined symmetries near U_1^z-U_1^z (0.5, 0, 0.15) at 4.26 eV, S_1-S_1 (0.3, 0.3, 0.5) at 4.27 eV, Δ_1-Δ_2 (0.36, 0, 0) at 4.26 eV, and an M_3 cp near (0.3, 0.1, 0.2) at 4.41 eV. The last structure we shall consider in the $\epsilon_2^{\parallel}$ spectrum occurs at 4.96 eV. This shoulder is caused in part by 20-28, 29 transitions in a region (mostly along the z direction) around (0.3, 0, 0.25) at 4.95 eV. Other contributions to this shoulder from critical points of undetermined symmetry are listed in Table VI.

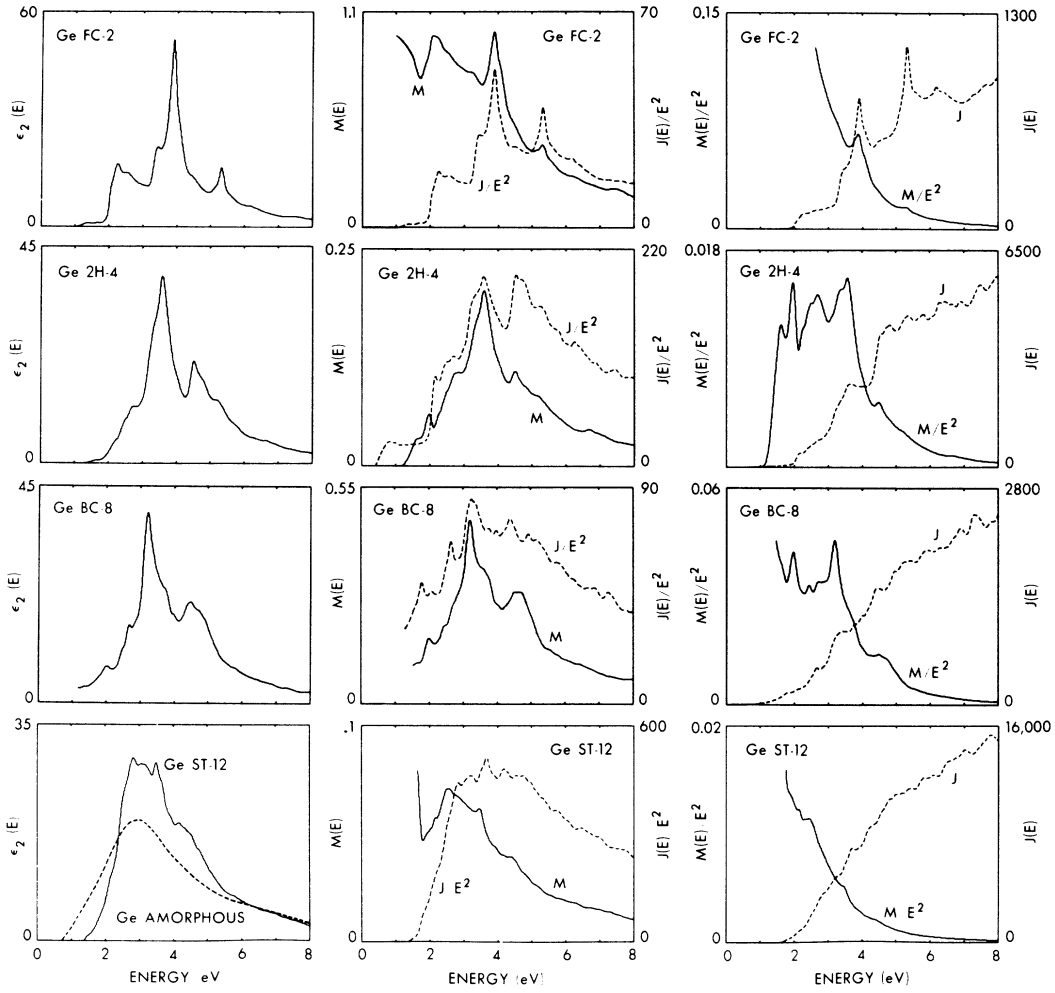

FIG. 13. Imaginary part of the dielectric function, ϵ_2, average gradient matrix element M, associated joint density of states J/E^2, average dipole matrix element M/E^2, and joint density of states J for Ge in the FC–2, 2H–4, BC–8, and ST–12 structures. For each row the product of the two curves in the second and third columns gives the ϵ_2 spectrum in the first column. The ϵ_2 for the 2H–4 and ST–12 structures was obtained by averaging over parallel and perpendicular polarizations. The matrix element M is in units of $(2\pi/a)^2$, where a is the smallest lattice constant of each crystal and J in the figure is in units of $(a/2\pi)^2$ eV^2. The unnormalized $J(E)$ defined in Eq. (3) can be obtained from the values of J in the figure by taking J to be in units of $(3\pi m^2/e^2\hbar^4)$ $(a/2\pi)^2/\mathrm{cm}^3$ eV. The amorphous ϵ_2 is from Donovan and Spicer (Ref. 4).

IV. DISCUSSION OF AMORPHOUS PHASES

The experimental amorphous dielectric function $\epsilon_2(E)$[4,5] (Figs. 13 and 14) consists of a seemingly featureless spectrum with one broad peak positioned near the Λ peak in the FC-2 ϵ_2. This spectrum is quite different from any known crystalline ϵ_2 (except for ST-12) and cannot be obtained by simply averaging the peaks in the FC-2 spectrum.

The theoretical attempts[10–15] to explain the amorphous ϵ_2 have all assumed that long-range disorder is of primary importance. They have taken the FC-2 band structure as a starting point and have applied various modifications to study the effect of long-range disorder. In some cases[10–14] complete $\vec{k}$ nonconservation was considered in the sense of a nondirect transition (NDT) and in other cases[11–13,15] partial $\vec{k}$ nonconservation was proposed which enabled the introduction of some type of short-range-order parameter. In all cases, however, the results are similar, in good agreement with experimental ϵ_2 data, and the authors agree that strong $\vec{k}$ nonconservation (long-range disorder) is a requisite in explaining the amorphous ϵ_2. None of these theories, however, predicts even a correct *trend* to the density of states of the amorphous phase. The single board peak[3] at the bottom of the valence-band density of states for the amorphous case is very striking and cannot be accounted for by a simple broadening of the two s-like peaks in the FC-2 structure. This problem was discussed in I, where we suggested that the experimental results could be explained by a short-range disorder which would make the presence of fivefold and sevenfold rings of bonds appreciable. It is precisely the lack of this short-range disorder in these theories that produces this inconsistency with the experimental data. To see this let us examine one of the most interesting and sophisticated of the aforementioned theories, which is that of a complex band structure (CBS).[13,15]

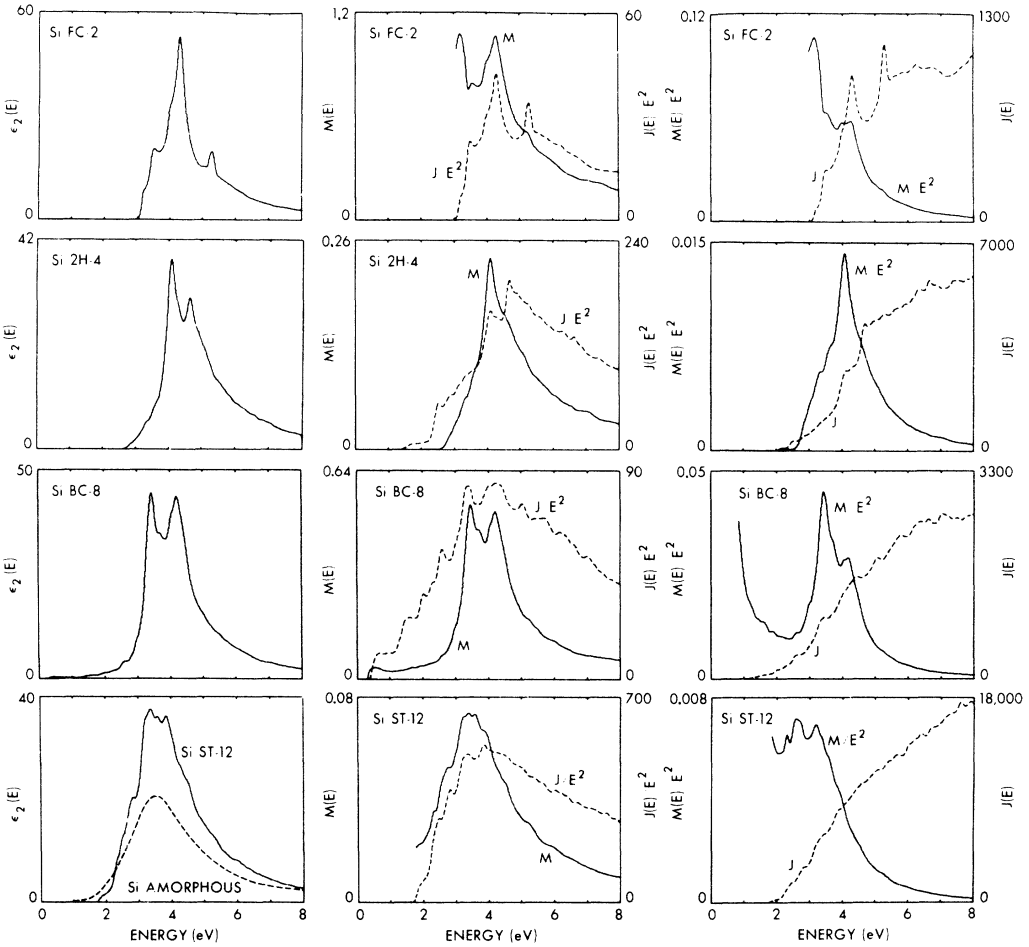

FIG. 14. Imaginary part of the dielectric function, ϵ_2, associated average matrix element M, associated joint density of states J/E^2, average dipole matrix element M/E^2, and joint density of states J for Si in the FC–2, 2H–4, BC–8, and ST–12 structures. The convention is the same as in Fig. 13. The amorphous ϵ_2 is from Pierce and Spicer (Ref. 5).

It was instigated by the work of Maschke and Thomas[12] and developed by Kramer. A one electron Green function is expanded in a Born series and a configurational averaging is applied by introducing in each term containing n scattering centers an n-particle correlation function which is integrated over all n sites. It is then assumed that the n-particle correlation functions can be approximated by products of two-particle correlation functions which are taken to be sums of Gaussian-like functions centered on lattice sites, with half-widths which increase with increasing distance from a given lattice point and are proportional to a small parameter α which describes the amount of disorder. This type of approximation treats correctly multiple scattering at one atom only, while higher multiple scattering terms are treated approximately correctly if one has $\alpha \ll 1$. The two-body correlation functions can be related to experimental amorphous radial distribution functions (RDF); however, we notice that in Ge, for example, it would be difficult to reproduce the second and third hump in the RDF[16] curves by simply placing Gaussian-like functions at FC-2 lattice points.

Nevertheless, the averaged Green-function series, which is written in terms of pseudopotentials $v(q)$,[17] can be reduced if one assumes slowly varying potential functions and small enough α so as to take $v(q)$ constant in the $\vec{k}$ integration, which in turn permits decoupling of terms and a resummation of the series. The poles of this averaged Green function are now obtained from a generalized pseudopotential secular equation which is now no longer Hermitian. Kramer then finds that he obtains complex energies whose real parts are approximately the energies of the crystal and whose imaginary parts can be interpreted as average reciprocal lifetimes or, equivalently, average energy widths. The average ϵ_2 spectrum is obtained by using the Kubo formula and performing a similar configurational averaging on a product of two one-electron Green functions. With some approximations the forms for the averaged ϵ_2 and density of states are similar in that they are written as a sum over partial spectra belonging to different regions of the BZ where the reciprocal lifetimes can be taken constant. The partial spectra are then given by a convolution of the *crystalline* spectrum (shifted in energy when appropriate as shown below) with a Lorentzian which depends on an average reciprocal lifetime. The parameter α was chosen to fit the ϵ_2 spectrum of amorphous Ge and Si.

Kramer's results show the valence band being affected very slightly while the conduction band is broadened considerably. In particular, for Ge the Γ_{25}-Γ_2 and L_1-L_3 gaps become smaller while the X_4-X_1 gap becomes larger. Furthermore, Γ_2 is very slightly broadened, L_2 is slightly broadened, and X_1 is largely broadened. This is not surprising nor difficult to understand. In principle, we would expect the electrons in the conduction band to be affected more by long-range disorder than the very-well-localized valence electrons. In fact, if we look at the charge density at symmetry points in the conduction band, we find that X_1 is largely spread out while L_3 is somewhat localized and Γ_2 shows definite signs of localization. This is exactly the same trend observed in the reciprocal lifetimes mentioned above. The effect of this on ϵ_2 is then to average out most of the X peak while preserving the Λ peak and shifting it to slightly lower energies. The agreement with the experimental amorphous ϵ_2 is good. The effect of Kramer's disorder on the density of states, however, is a strong averaging of the conduction band and a very small averaging of the valence-band peaks for FC-2. This is certainly not in agreement with experiment.[3] The problem is that one is dealing here with a system that has the short-range order of diamond. In fact, the parameter α, used to fit ϵ_2, is very small and corresponds, for example, to all first, second, and half the third nearest neighbors being within a deviation of only $0.04a$ of the crystalline FC-2 positions. It could be suggested that the density of states might agree better with experiment if α was taken to be larger. But now the ϵ_2 would be shifted to lower energies and agreement with experiment here would be considerably marred. Besides, the approximations involved in obtaining Kramer's final expressions may not be valid for large α.

Thus we believe that the conclusions drawn by applying the CBS theory to the FC-2 structure are not valid for the amorphous case. The suggestion[18] that the peak in the amorphous ϵ_2 is due to Λ transitions because of the preservation of the bonding direction is questionable and is only supported by analyzing a hypothetical "amorphous" system that is too close to the FC-2 structure.

The results from these theories lead us to suspect that the ϵ_2 spectrum may not be a good judge of the microscopic structural aspects of the amorphous state and that one needs a theory that will be able to account for *both* the density of states and ϵ_2 in the amorphous phase. In I, we applied the concept of short-range disorder to the density of states and obtained good agreement with experiment. We shall now do the same for the ϵ_2 spectrum.

There are two features of the amorphous ϵ_2 spectrum which are of primary importance. These are, of course, the one-hump form of the spectrum and the position in energy of this hump. We shall attempt to account for these features in the following analysis.

The crystalline $\epsilon_2(E)$ may be written as

$$\epsilon_2(E) = CJ(E) \sum_{\vec{k}} \sum_{c,v} \delta(E_c(\vec{k}) - E_v(\vec{k}) - E)$$

$$\times |\langle \psi_c(\vec{k}) | \vec{r} | \psi_v(\vec{k}) \rangle|^2 / J(E) , \quad (2)$$

where C is a constant and $J(E)$ is the joint density of states given by

$$J(E) = \sum_{\vec{k}} \sum_{c,v} \delta(E_c(\vec{k}) - E_v(\vec{k}) - E) . \quad (3)$$

Equation (2) is just an expression for an average matrix element $P(E)$ multiplied by the joint density of states $J(E)$. If we now incorporate the constant C into $J(E)$ we can write

$$\epsilon_2(E) = J(E) P(E) . \quad (4)$$

This is a physically reasonable expression and could be used to study the amorphous phase since it is essentially the number of states accessible for transitions at an energy E, multiplied by an average probability for those transitions. When one does band-structure calculations, however, it is easier to calculate an associated average matrix element $M(E)$ obtained by a weighted averaging of $|\langle \psi_c(\vec{k}) | \vec{\nabla} | \psi_v(\vec{k}) \rangle|^2$. Then Eq. (3) can be written as[19]

$$\epsilon_2(E) = J(E) M(E) / E^2 . \quad (5)$$

Equation (3) or (4) can now be used to qualitatively account for the amorphous ϵ_2 spectrum in a simple way. In the amorphous case we would expect $J(E)$ to be a monotonically *increasing* function of energy without any sharp structure from specific localized regions in the BZ. Similarly we would expect the average dipole matrix element $P(E)$ to be a smooth monotonically *decreasing* function of energy. The product of these two functions would then give a one-hump structure which would explain the shape of the amorphous ϵ_2. To examine this in more detail we have calculated ϵ_2, J/E^2, and M, and J and M/E^2, as functions of energy for Ge and Si in the FC-2, 2H-4, BC-8, and ST-12 structures using the Gilat-Raubenheimer[9] integration scheme. The results are shown in Figs. 13 and 14. For each row the product of the two curves in the second and third columns gives the ϵ_2 spectrum in the first column. In the cases of 2H-4 and ST-12 structures we show the weighted average of the parallel and perpendicular components of ϵ_2. We are interested in observing the trends as we go from FC-2 down the columns to more and locally disordered and complicated crystal structures. For the moment let us concentrate on the third column in each figure. We notice that with the increasing complexity of the crystal structures, J gradually loses the sharp structure prominent in the FC-2 case, which was caused by the simplicity and symmetry of this band structure. When we reach ST-12, J is almost a smooth and featureless spectrum which would compare well with what we expected in the amorphous case. In addition the average dipole matrix element M/E^2 for ST-12 is for the most part a smooth decreasing function of energy. This is particularly the case for Ge ST-12 in a large energy region, while in ST-12 this is true for $E > 3$ eV, which, however, contains the peak of ϵ_2. If we now examine the ϵ_2 spectra we notice that it is precisely the ST-12 structure that has the qualities of the superimposed amorphous ϵ_2 spectrum obtained by Donovan and Spicer[4] for Ge and by Pierce and Spicer[5] for Si. The agreement between the ST-12 spectra and the amorphous spectra is quite encouraging and shows that the kind of short-range disorder[1] which accounted for the amorphous density of states also accounts for the important features of the amorphous ϵ_2 spectrum. The discrepancy in magnitude of the ϵ_2 curves is irrelevant in this discussion and is caused in part by the differences in bulk density of the ST-12 and amorphous structures.

An interesting feature that comes out of this analysis is that J/E^2 should look something like a step function in the amorphous case since J is such a smooth polynomiallike increasing function of energy. This would then suggest that the average gradient matrix element M must contain most of the information about ϵ_2. This is shown in Figs. 13 and 14 as we go down the second column, where we have plotted J/E^2 and M. In the FC-2 case the ϵ_2 spectrum looks mostly like J/E^2, while M simply modulates the J/E^2 spectrum. In the 2H-4 structure we find that the form of the ϵ_2 spectrum is now shared between J/E^2 and M, where M contributes most of the first peak and J/E^2 contributes the second peak. When we examine the BC-8 case we find that the ϵ_2 spectrum now looks mostly like M while J/E^2 just modulates the M spectrum. Finally, in the ST-12 structure we find that J/E^2 is a relatively featureless steplike function of energy and again ϵ_2 looks like M.

Therefore, we can safely conclude from this that the average gradient matrix element M determines the position in energy of the hump in the amorphous ϵ_2, and most important, when one measures the amorphous ϵ_2 spectrum, one is essentially just measuring the average matrix element M.

V. CONCLUSIONS

Our aim in this work has been twofold. First, to make a complete band-structure analysis of Ge and Si in a series of novel, interesting, and complicated crystal structures. This included calculating energy eigenvalues, densities of states, and optical functions, determining the symmetry of wave functions, and identifying optical structure. Second, to use the increasing complexity of the crystal structures to study the trends observed in the density of states and the imaginary part of the dielectric function as we approach the amorphous phase. To this end we have made particular use of the ST-12 structure which has deviations in bond lengths and angles

and has odd-numbered rings of bonds. We have not used the ST-12 structure as a replica of amorphous Ge and Si, but rather as a tool to probe the important microscopic structural aspects of the amorphous phase.

We have found that if one is to make a reliable model of the amorphous phase, one cannot start with a *long-range-disorder model* applied to the FC-2 structure. On the other hand, a *short-range-disorder model*, defined as a system with deviations in bond angles and bond lengths, with all bonds satisfied, and with odd-numbered rings of bonds, could account for *both* the amorphous density of states and imaginary part of the dielectric function. In particular we found that the amorphous ϵ_2 is just the spectrum of an average matrix element.

If we now include *long-range disorder* to our *short-range disorder*, we would expect to have a much better model for the amorphous phase. Our point is, however, that the effects of long-range disorder are of *secondary* importance.

---

*Supported in part by the National Science Foundation under Grant No. GH 35688.

[1]J. D. Joannopoulos and M. L. Cohen, Phys. Rev. (to be published).

[2]The optical properties and density of states of Ge $2H$-4 has also been calculated by I. B. Ortenburger, W. E. Rudge, and F. Herman, J. Non-Cryst. Solids **8**, 653 (1972).

[3]L. Ley, S. Kowalczyk, R. Pollak, and D. A. Shirley, Phys. Rev. Lett. **29**, 1088 (1972).

[4]T. M. Donovan and W. E. Spicer, Phys. Rev. Lett. **21**, 1572 (1968).

[5]D. T. Pierce and W. E. Spicer, Phys. Rev. B **5**, 3017 (1972).

[6]J. S. Kasper and S. M. Richards, Acta Crystallogr. **17**, 752 (1964).

[7]A. W. Luehrmann, thesis (University of Chicago, 1967) (unpublished).

[8]J. Zak, A. Casher, M. Glück, and Y. Gur, *The Irreducible Representation of Space Groups*, edited by J. Zak (Benjamin, New York, 1969).

[9]G. Gilat and L. J. Raubenheimer, Phys. Rev. **144**, 390 (1966).

[10]F. Herman and J. P. Van Dyke, Phys. Rev. Lett. **21**, 1575 (1968).

[11]D. Brust, Phys. Rev. Lett. **23**, 1232 (1969).

[12]K. Maschke and P. Thomas, Phys. Status Solidi **39**, 453 (1970).

[13]B. Kramer, Phys. Status Solidi **41**, 649 (1970).

[14]K. Maschke and P. Thomas, Phys. Status Solidi **41**, 743 (1970).

[15]B. Kramer, Phys. Status Solidi **47**, 501 (1971).

[16]D. E. Sayers, E. A. Stern, and F. W. Lytle, Phys. Rev. Lett. **27**, 1204 (1971).

[17]M. L. Cohen and T. K. Bergstresser, Phys. Rev. **141**, 789 (1966).

[18]J. Stuke, J. Non-Cryst. Solids **4**, 1 (1970).

[19]A similar expression has also been used by Maschke and Thomas (Ref. 14).